O. E. LIBRARY

DATA LIBRARY
Woods Hole Oceanographic Institution

R 686

Technical Report

# STRUCTURAL DESIGN OF CONICAL ACRYLIC VIEWPORTS

June 1970

Sponsored by

NAVAL FACILITIES ENGINEERING COMMAND

NAVAL CIVIL ENGINEERING LABORATORY

Port Hueneme, California

This document has been approved for public release and sale; its distribution is unlimited.

TA
417
.N3
no.R686

# STRUCTURAL DESIGN OF CONICAL ACRYLIC VIEWPORTS

Technical Report R-686

YF 38.535.005.01.005

by

M. R. Snoey and M. G. Katona

## ABSTRACT

The purpose of this report is to establish a rational engineering approach for the design of conical acrylic viewports. To achieve this goal, a time-dependent, yield-failure criterion was developed and utilized in the analysis of a variety of viewport configurations. Specifically, a range of thickness/minor diameter **(t/d)** ratios from 0.25 to 1.75 and included angles from $60^{o}$ to $120^{o}$ were analyzed by the finite element technique. Using the viewport structural analysis in conjunction with the yield-failure criterion for acrylic, time-dependent operating depths were determined as a function of viewport configuration.

Paralleling the above, an experimental investigation was performed to validate the analytical results. Six full-scale viewports were tested for a year under simulated operational conditions that included simultaneous cycling of pressure and temperature, 0 to 4,000 psi and 70 to $35^{o}$F, respectively.

Comparison of analytical and experimental results indicated excellent agreement for the physical location of viewport failure at specified loading histories.

Design recommendations are presented in the form of design curves which enable the design of a conical acrylic viewport for a specified operating pressure and duration under load. To complete the recommendations, design information is given also on sealing with a conventional O-ring, as well as guidelines for elevating a viewport in its flange.

This document has been approved for public release and sale; its distribution is unlimited.

Copies available at the Clearinghouse for Federal Scientific & Technical Information (CFSTI), Sills Building, 5285 Port Royal Road, Springfield, Va. 22151

O. E. LIBRARY

CONTENTS

page

INTRODUCTION ..... 1
Objectives ..... 1
Purpose ..... 1
SCOPE OF INVESTIGATION ..... 3
Experimental Phase ..... 3
Analytical Phase ..... 5
General ..... 5
Concept of Failure ..... 5
Method of Analysis ..... 6
RESULTS AND DISCUSSION ..... 8
Experimental ..... 8
Post-Test Observations ..... 11
Displacements ..... 14
Analytical ..... 14
Stresses ..... 14
Displacements ..... 16
Comparison of Experimental and Analytical Results ..... 16
Discussion ..... 24
FINDINGS ..... 25
DESIGN RECOMMENDATIONS ..... 27
Design Curves ..... 27
Material ..... 27
Structure ..... 28
Example ..... 30
ACKNOWLEDGMENT ..... 31

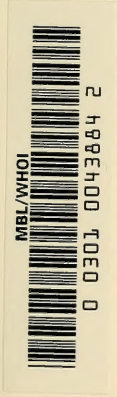

page

APPENDIXES

A—Investigation of a Viewport Seal Design . . . . . 32

B—Equipment and Procedure for Experimental Phase . . . . . 41

C—Failure Criterion Applied to Conical Acrylic Viewports . . . 47

REFERENCES . . . . . 53

LIST OF SYMBOLS . . . . . 55

## INTRODUCTION

### Objectives

1. Accumulate experimental test data on full-scale viewports under simulated operational conditions.
2. Develop a rational failure criterion for conical acrylic viewports.
3. Develop parametric design curves based on the failure criterion.

### Purpose

The presence of viewports in practically every undersea vehicle is indicative of their importance for visibility in undersea research. Piccard[1] first introduced conical acrylic viewports in 1939 and, presently, 18 submersibles, or about half the total number, utilize Piccard's $90^{o}$ conical frustum design for a wide range of operating depths. Figure 1 shows full-scale, $90^{o}$ conical viewports while Reference 2 contains a historical background on viewports along with a summary of viewport designs for about 40 vehicles.

This study is intended to satisfy a need in the design of conical viewports that has existed and has seen no improvement for the past 30 years. The need was to develop parametric design curves based on the viewports functional use and to include time effects (creep) in the design curves.

A thorough structural analysis of a conical viewport was not even available until just recently.[3,4,5] All three of these references provide good insight into the structural response of a conical viewport, however, they do not provide any information for the designer.

Although acrylic viewports have accumulated a large amount of operational time, thereby generating some confidence in the material, trepidations still do exist. Design curves based on accurate experimental material tests, a rational failure theory, and complete structural analysis should relieve these fears and provide more confidence in viewport design.

Design recommendations for conical acrylic viewports would not be complete without a section on sealing. Therefore, Appendix A contains information on methods of sealing and how they affect the viewport design economically, operationally, and structurally.

Figure 1. Full-scale, 90° conical acrylic viewports.

## SCOPE OF INVESTIGATION

The investigation was divided into two sections: (1) the experimental phase which will be discussed first followed by (2) the analytical phase.

### Experimental Phase

The objective of the experimental tests was to accumulate data on full-scale, $90^{o}$ conical viewports with a range of thickness to minor diameter ratios, **t/d**. Figure 2 shows a cross section of a typical viewport. The test conditions simulated actual operational conditions as nearly as possible so that the results could be used to provide insight on the type and location of failures occurring during operation. More importantly, the data would serve to test the validity of the analytical results.

Tests were conducted on six viewports of three sizes as listed in Table 1. The viewports were all machined from a 4-inch-thick commercial cast sheet of Plexiglas G acrylic plastic. The minor diameters were approximately 4, 6, and 8 inches which gave **t/d** ratios of 0.92, 0.61, and 0.45, respectively.

Table 1. Full-Scale Experimental Viewport Dimensions

| Included Angle, $\alpha$ (±5′) | Major Diameter, D (in.) | Minor Diameter, d (in.) | Thickness, t (in.) | t/d |
|---|---|---|---|---|
| $90^{o}$ 0′ | 11.863 | 4.193 | 3.835 | 0.915 |
| $90^{o}$ 0′ | 11.854 | 4.180 | 3.837 | 0.916 |
| $90^{o}$ 0′ | 13.969 | 6.299 | 3.835 | 0.610 |
| $90^{o}$ 0′ | 13.950 | 6.292 | 3.829 | 0.608 |
| $90^{o}$ 0′ | 16.013 | 8.411 | 3.801 | 0.453 |
| $90^{o}$ 0′ | 16.025 | 8.431 | 3.797 | 0.451 |

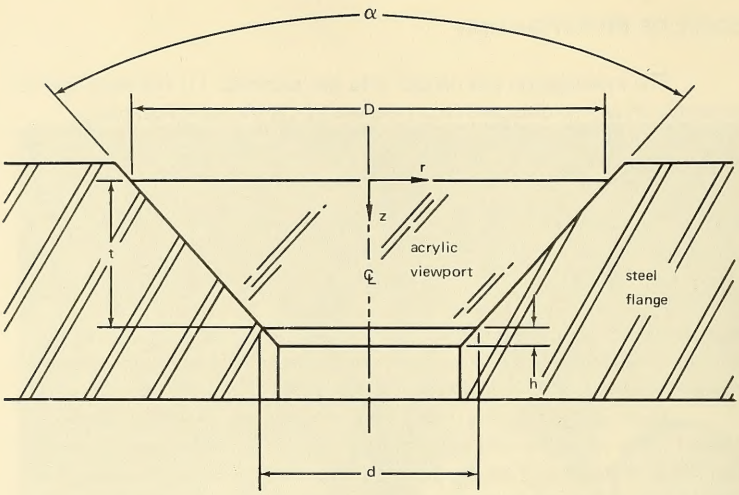


Figure 2. Cross section of a typical viewport.

The six viewports were tested simultaneously in three refrigerated pressure vessels. Displacements and post-test observations served as the recordable data. Details on the equipment and test procedure used are in Appendix B.

Inasmuch as an undersea vehicle might make many dives, cycling of the pressure load was included as part of the test procedure. The simulation of actual dives required simultaneous changes in pressure and temperature. As the pressures were changed from 0 to 4,000 psi, the temperature simultaneously was changed from 70 to 35°F. It was believed that the most severe test of the viewports would be to cycle the maximum creep strains occurring in each viewport under the 4,000 psi load. Therefore, the period of the cycle for all viewports was determined by loading the least conservative design, $t/d = 0.45$, and letting the viewport displace until the displacement-time curve was asymptotic within the accuracy of the measuring system. This resulted in a "load-on" time period of 500 hours with a "load-off" or relaxation period of 100 hours; the time necessary to completely relax all the strains so the viewport would return to zero displacement. The tests were conducted over a 1-year period which resulted in 13 total cycles.

## Analytical Phase

**General.** The knowledge gained from the experimental tests was utilized as a basis for performing an analytical study on viewport designs. In particular, analytical investigation for a spectrum of viewport parameters, t/d and $\alpha$ ranging from 0.25 to 1.75 and $60^{o}$ to $120^{o}$, respectively, was accomplished by means of the finite element technique.

In order to develop rational design recommendations, it is necessary to define the capacity of the system, i.e., what constitutes failure. Since the failure mode definition and failure criteria influence the assumptions made in an analytical study, the concept of failure is discussed prior to the analytical method of attack.

**Concept of Failure.** Failure must be considered from two viewpoints: (1) the structural level and (2) the material level. First, at the structural level, the investigator must define failure. In the past, structural viewport failure has been taken as the complete collapse of the system, often called the upper limit or ultimate strength, which is typified by large plastic flow and rupture. Another definition of failure is the lower limit capacity of a system which is defined as that load which causes initial plastic yielding in any local region of the system.

The authors have chosen the lower limit or "yield criterion" as the definition for failure of acrylic viewports based on the following considerations. (1) The functional use of a viewport is to transmit undistorted and undiminished light to the viewer, however, earlier experimental results have shown that this function is seriously impaired when the viewport is loaded into the plastic range which results in crazing and distortion of the acrylic. (2) The pressure that causes yielding is much lower than the load causing ultimate collapse failure, consequently, a built-in safety factor for the hazardous environment is intrinsic in the lower limit design, in addition to the standard safety factor used for the functional aspect.

The second major consideration in establishing a failure criterion belongs to the realm of the material itself independent of the particular structure configuration and functional use.

Since, by definition, the structure fails when local yielding occurs, this dictates that a yield criterion for acrylic must be established which will adequately predict yield states under combined stresses. Fortunately, much research has been accomplished in this area and it has been shown that the Huber-von Mises-Hencky or distortion energy theory of failure[6] predicts combined-stress yield-states extraordinarily well for acrylic.[7,8] However, this flow law is complicated by the anisotropic response of yielding in tension

and compression with tensile strength being lower than the compressive. A conservative approach was used to circumvent this problem. The tensile strength was applied to combined states of stress at any time when at least one principal stress was significantly in a tension zone, and the higher compressive strength was used strictly in the all-compression failure octant.

Because acrylic is a typical thermoplastic, two additional variables significantly affect its material properties: temperature and time.

In general, when temperatures are increased, acrylic material properties decrease in value. This feature of acrylic makes it an ideal material for its proposed use as a viewport for an undersea vehicle because the ocean provides a low-temperature environment which enhances properties over those measured at room temperature.

The design recommendations set forth in this report are based upon material response at room temperature, thus allowing the additional strength of the acrylic due to lower temperatures at operational depths to increase the margin of safety.

The second variable, time, is not as easily dealt with as temperature, but is certainly important due to the creep properties of acrylic. For this reason every effort has been made to rationally treat the effect of time on the stress distributions of the viewport and the yield strength of the acrylic. The details of this approach are given in Appendix C as a separate topic because this treatment is not limited to viewports; the approach may be used for any structure utilizing acrylic.

Briefly, the approach is to choose the "worst" stress distribution and utilize this for any value of the parameter time, while the development of a yield-stress versus load-duration curve provides the factor of time in the design parameters. Appendix C deals with the concepts in a straightforward and rational manner.

**Method of Analysis.** As discussed in Appendix C, the highest stress concentrations result from the viscoelastic solution when time is equal to zero. This is identical to elastic solutions; consequently, elastic solutions based on all the classical assumptions of linear, infinitesimal-strain, elastic theory were assumed and the solutions were obtained by the finite element program for an axisymmetric solid written by Wilson.[9] References 4 and 5 verify the capability of using a finite element analysis on conical acrylic viewports.

The sequence of analysis was as follows: for each viewport configuration, the finite element program computed the local state of stress at every element and the corresponding effective stress defined as

$$\sigma_o = \sqrt{\frac{(\sigma_1 - \sigma_2)^2 + (\sigma_2 - \sigma_3)^2 + (\sigma_3 - \sigma_1)^2}{2}}$$

where $\sigma_o$ = effective stress at an element per unit of applied pressure

$\sigma_1, \sigma_2, \sigma_3$ = principal stresses at each element per unit of applied pressure

Thus the relationship for yielding becomes

$$p = \frac{\sigma_y}{\sigma_o}$$

where

**KNOWN BY FINITE ELEMENT SOLUTION**

- $\sigma_o$ = the maximum effective stress of all elements with all the principal stresses in compression

or

- $\sigma_o$ = the maximum effective stress of all elements with any tension in the principal stresses

**KNOWN BY YIELD-STRESS VS TIME CURVES**

- $\sigma_y$ = material yield strength in compression for a particular loading duration

or

- $\sigma_y$ = material yield strength in tension for a particular loading duration

**DESIGN REQUIREMENT**

- p = the maximum pressure that can be applied to the viewport which initiates yielding in any zone with all the principal stresses in compression

or

- p = the maximum pressure that can be applied to the viewport which initiates yielding in any zone with tension in the principal stresses

The above format explicitly sets forth the procedure used to determine the capacity of the various viewport geometries.

A further point of concern was in specifying the boundary condition between the viewport and the flange. In order to account for all practical contingencies, two extreme boundary conditions were applied to each viewport configuration as shown in Figure 3: (1) the boundary was fixed, representing maximum friction between the acrylic viewport and its flange; and (2) the boundary was allowed to be frictionless, representing perfectly smooth, greased interfacing. Of these two boundary conditions, the one resulting in the controlling failure as outlined above, was chosen as the governing boundary condition.

A structural response discovered during the course of the analysis was that an arbitrarily high stress concentration existed in the element at the corner of the low-pressure face for all viewport configurations and boundary conditions. This phenomenon correlated with experimental findings where it was discovered that the low-pressure face corner underwent deformation or "rounding" for even the smallest load magnitudes (see Figure 4).

An intensive analytical investigation, outlined in Appendix C, revealed that the spiked stress concentration was relieved by deforming the corner of the mathematical model as was suggested by the experimental models. Thus, the viewport geometries considered in this report were all analyzed with a predeformed corner characterizing an actual viewport after its initial loading.

The last analytical refinement considered was to investigate the response from an O-ring groove machined in the acrylic. The analytical results along with the experimental tests are presented in Appendix A.

Input to Wilson's code[9] required material properties for acrylic. Reference 5 describes experimental tests performed to determine these necessary values at room temperature as: modulus of elasticity, 444,000 psi; and Poisson's ratio, 0.4.

## RESULTS AND DISCUSSION

### Experimental

Post-test visual observations and displacements at the center of the viewport low-pressure face served as experimental data. Since the viewports were all exposed to the same pressure loading and environment, the cause of any post-test effects would be the differences in structural design (all other variables considered equal).

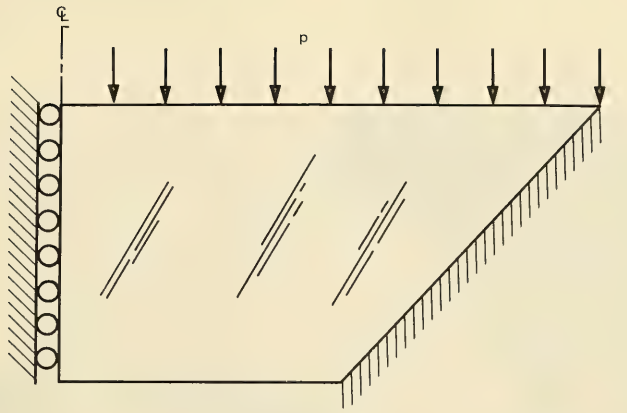


(a) Fixed boundary.

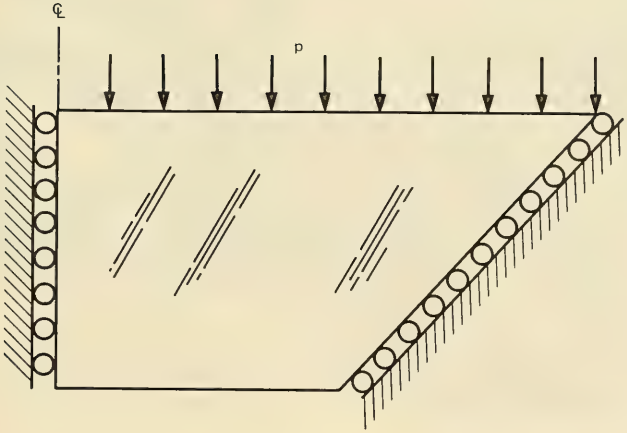


(b) Free boundary.

Figure 3. Boundary conditions for finite element analysis.

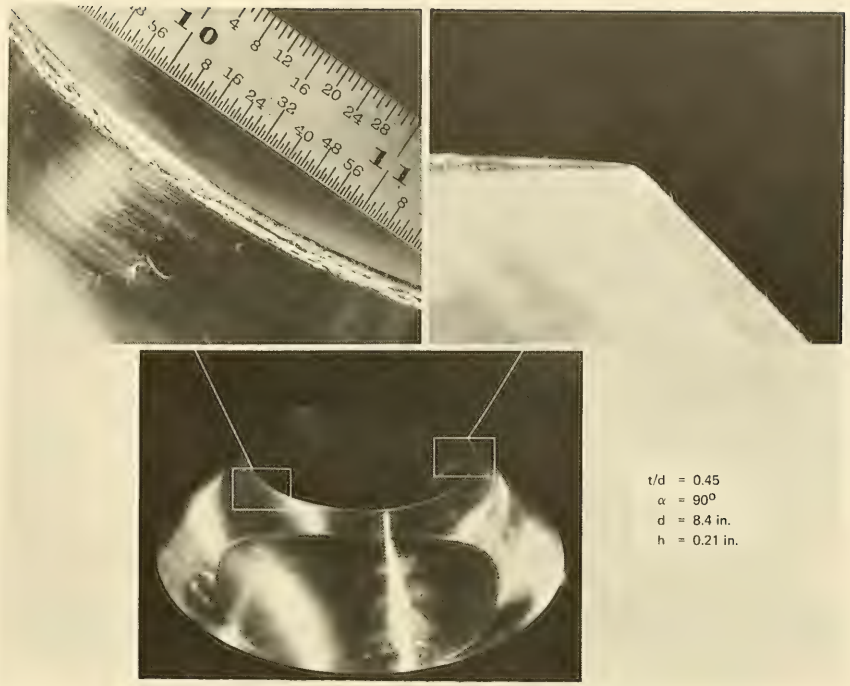


Figure 4. Post-test physical condition of t/d = 0.45 viewport after thirteen cycles.

**Post-Test Observations.** Failure results on the six viewports are contained in Table 2. From Table 2, it is shown that as the **t/d** ratio decreased, the frequency of stress crazing and cracks increased. Figures 4, 5, and 6 provide a visual supplement to Table 2. The least conservative design or the lowest **t/d** ratio (0.45) is shown in Figure 4. The resulting cracks and deformation at the low-pressure face corner are clearly shown. There was no visible damage anywhere else on the viewport. Collection of condensate around the low-pressure face resulted in an accumulation of rust on the flange which caused the ragged surface on the rounded corner of the viewport.

Table 2. Results of Test on Full-Scale Viewports

| **t/d** Ratio | Maximum Width of Crack Pattern (in.) | $\frac{\text{Creep Displacement}}{\text{Total Displacement}} \times 100$ (%) |
|---|---|---|
| 0.92 | 0<br>0 | 14 |
| 0.61 | 1/16<br>0 | 20 |
| 0.45 | 3/32<br>1/16 | 26 |

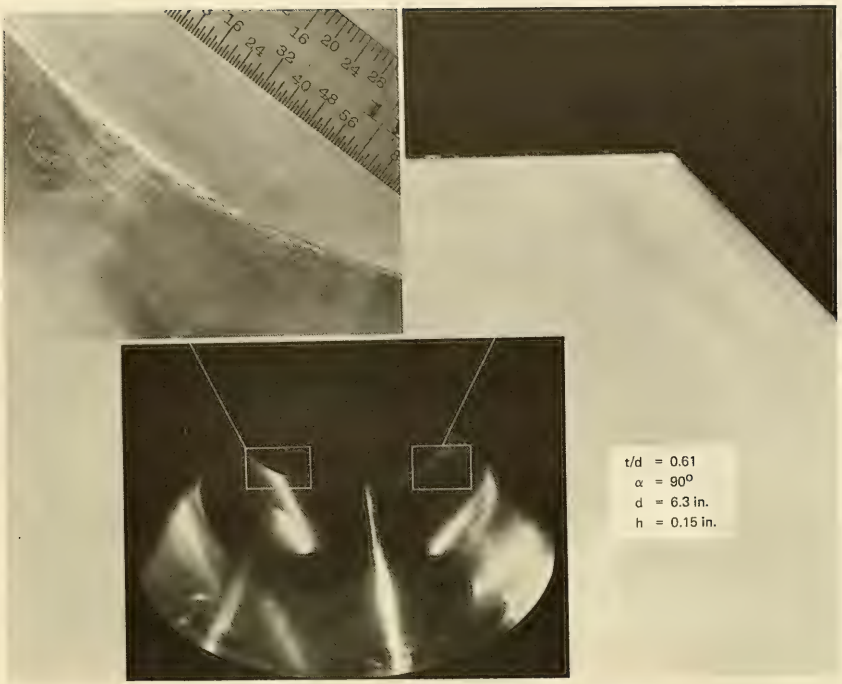


Figure 5. Post-test physical condition of t/d = 0.61 viewport after thirteen cycles.

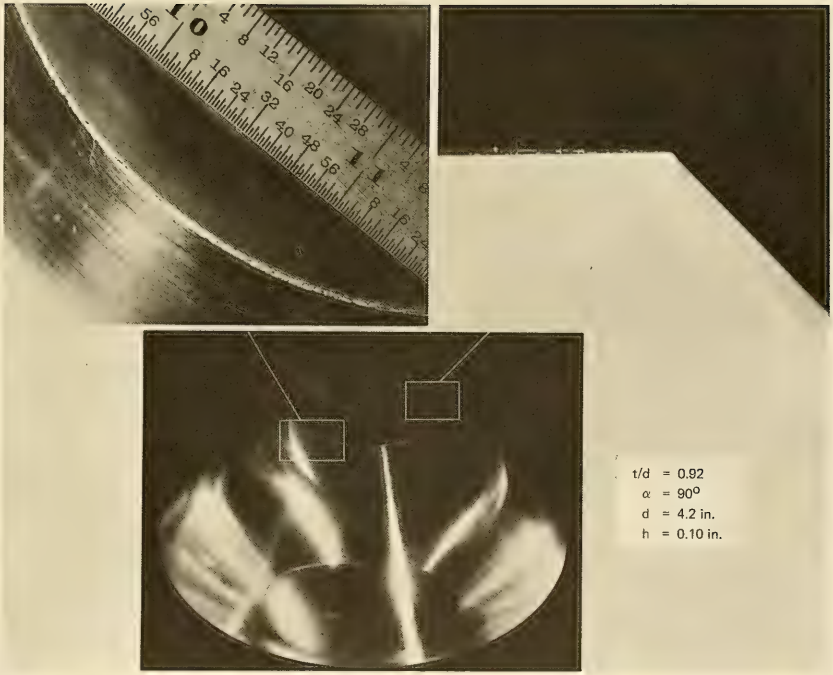


Figure 6. Post-test physical condition of t/d = 0.92 viewport after thirteen cycles.

The **t/d** = 0.61 viewport with its crazing cracks is shown in Figure 5. These cracks are much smaller than the ones in Figure 4 and the crack band is much narrower. The corner did not deform as much as in the previous case.

In the most conservative design, **t/d** = 0.92, there were no cracks visible anywhere. In fact, the corner rounding even appeared to be at a minimum.

**Displacements.** Figure 7 contains the absolute displacements of the three pairs of experimental viewports which are presented in this case to provide the designer with a good feel for maximum viewport displacements. The pressure and temperature cycling periods are also shown in Figure 7. Table 2 gives the percentage of the total displacement due to creep.

To simulate a dive, the pressure was increased at a rate of 50 psi/min, and the cooling of the system was initiated. It should be noted that at the operating depth or highest pressure, the temperature is the lowest. The total time period for a typical cycle was 600 hours. As was expected, the least conservative design, **t/d** = 0.45, had the highest absolute displacement (Figure 7) and the highest percentage of creep (Table 2).

### Analytical

Analytical results consist of pertinent plots and data extracted from the finite element analysis results. The data are divided into two areas: (1) stresses and (2) displacements. Both results demonstrate the variations in structural response due to changes in the following parameters: **t/d** ratio, included angle, and boundary condition.

**Stresses.** Figures 8 through 13 include both a contour and surface plot of the effective stresses for each of the 24 computer runs; four **t/d** ratios, three included angles, and two boundary conditions were used. The stress contour plots provide visual quantitative data, whereas, the surface plots provide visual qualitative data. Figures 8, 9, and 10 present the results for the fixed boundary condition, and Figures 11, 12, and 13 present the results for the free boundary case. In all of the plots, the stress concentration is apparent at the corner of the low-pressure face. For either the fixed or free boundary condition, the strength of the viewport is seen to increase with an increase in either the **t/d** ratio and/or the included angle. This agrees with data developed in Reference 3.

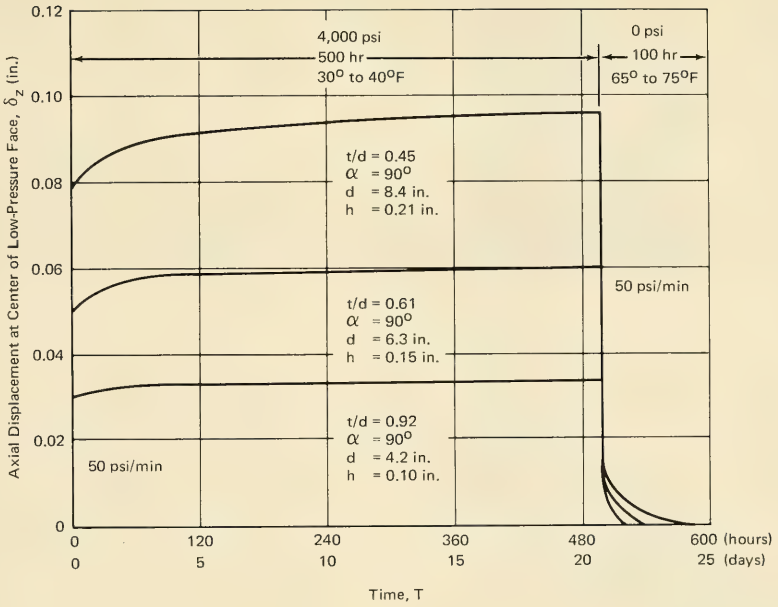


Figure 7. Typical displacement responses during one of thirteen cycles.

Two items of interest are apparent from the surface plots: (1) the flexural bending behavior exhibited by the **t/d** = 0.25 viewports and the absence of bending exhibited by the **t/d** ratios of 0.75, 1.25, and 1.75; and (2) the absence of high effective stresses at the high-pressure face corner. Generally speaking, this latter area appears to be in almost a hydrostatic stress state which means that some structural modification could be made in this region (refer to Appendix A).

**Displacements.** Figure 14 illustrates the displacements at the center of the low-pressure face. The results are presented in nondimensional form for use with any diameter viewport. Generally speaking, the difference in displacement between the fixed and free boundary condition is the gross distance that the viewport moves. Thus, the $60^{o}$ included angle viewport displaces much more in the free case, which causes the higher effective stress at the low-pressure face corner. The $90^{o}$ and $120^{o}$ viewports displace less and thus, the effective stress is less. The transition to flexural behavior is evident in Figure 14 by the knee in the curve at about **t/d** = 0.6. Two additional points (**t/d** = 0.45) from the analysis in Appendix A are included in Figures 14, 15, 16, and 17.

Figure 14 is also used in the Design Recommendations section of the report for calculating elevation of the viewport in the flange.

### Comparison of Experimental and Analytical Results

Figures 15 and 16 provide a comparison of experimental and analytical results. Figure 15 is based on the operating pressure and shows an excellent comparison. The experimental data is based on post-test observations of the six experimental viewports, while the analytical data is based on the magnitude of the effective stress at the low-pressure face corner. Cracks determined the presence of failure in the experimental viewports, while the controlling factor in the analytical analysis was the pressure required to equate effective stress with yield stress in the compression-compression-compression octant. Note that the free boundary condition controls for the range of the **t/d** ratios and that the analytical curves were shifted to the left by 20% in accordance with the low temperature.[4,10] Although the $35^{o}$F sea water is on the high-pressure face, it is a fair assumption that the steel flange has a low-temperature-gradient throughout and thus, provides a $35^{o}$F interface with the viewport.

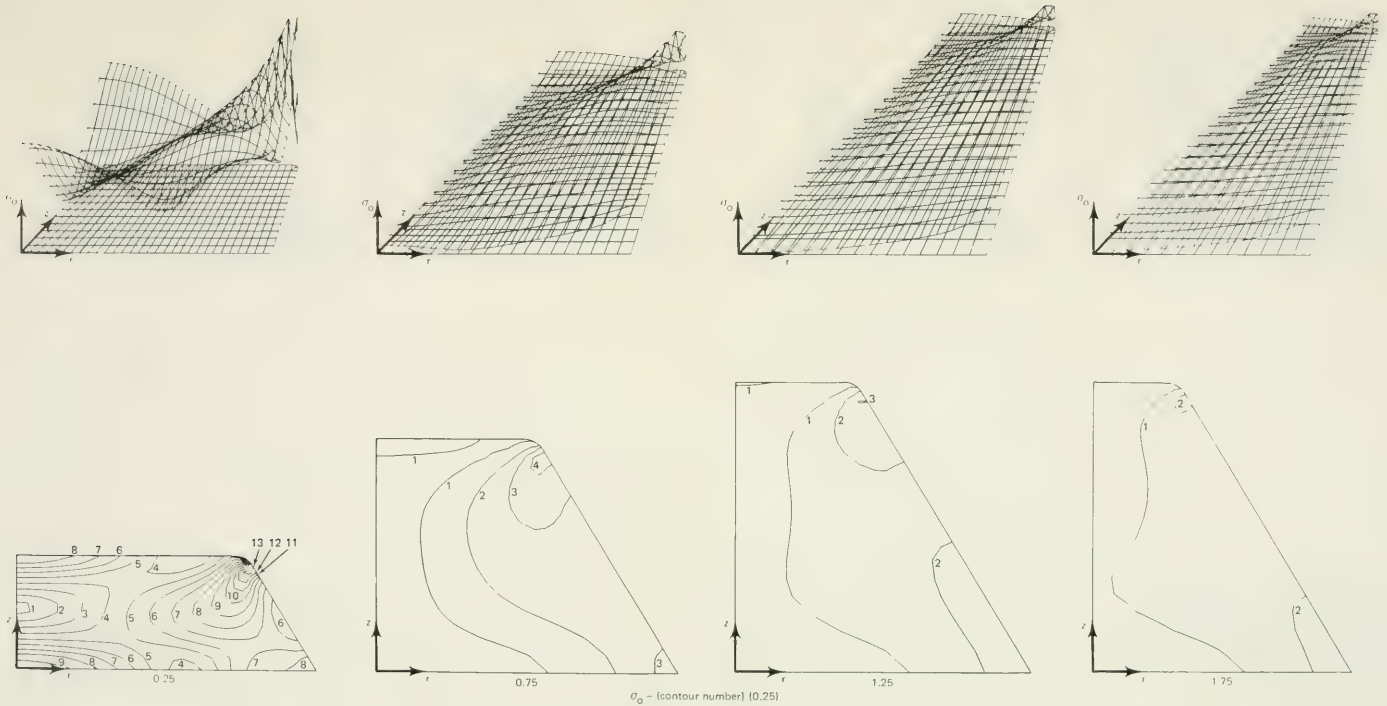


Figure 8. Effective stress contour and surface plots for 60° angle and fixed boundary condition.

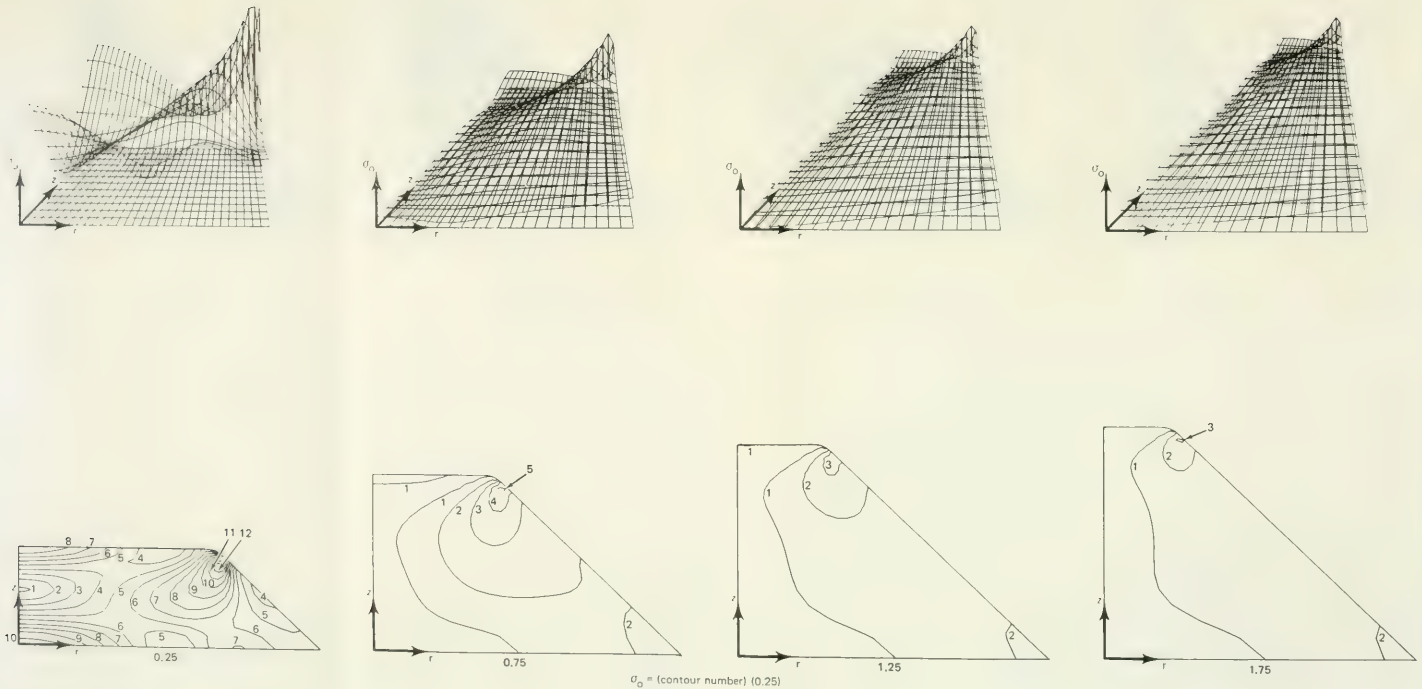


Figure 9. Effective stress contour and surface plots for 90° angle and fixed boundary condition.

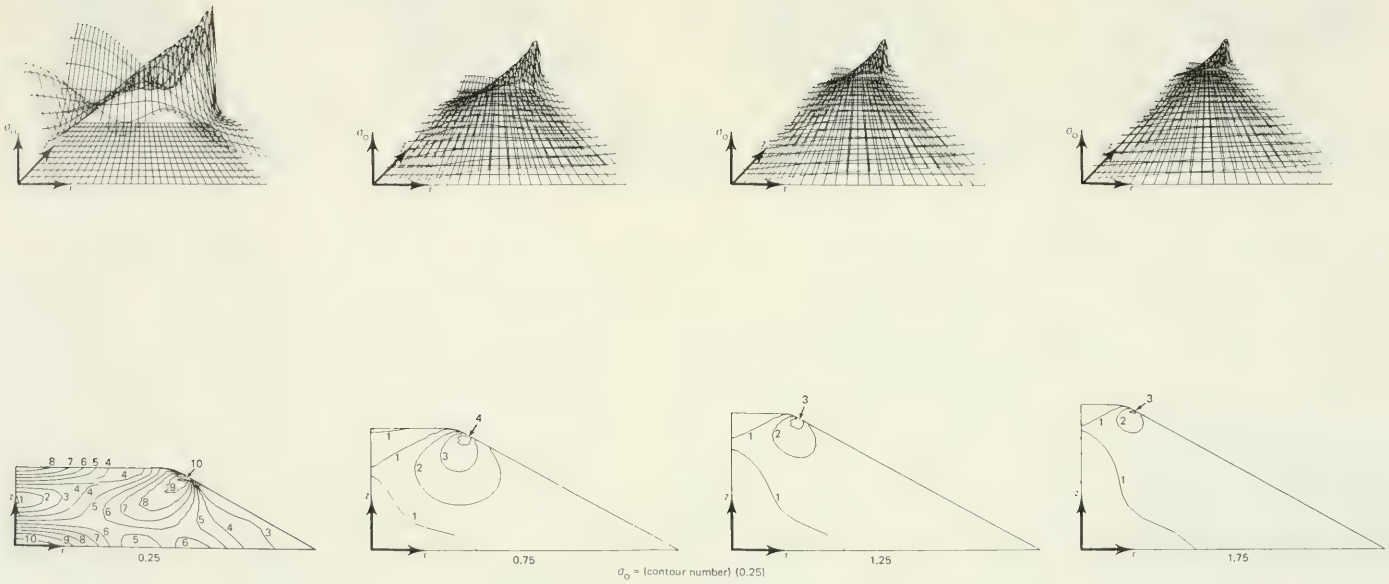


Figure 10. Effective stress contour and surface plots for 120° angle and fixed boundary condition

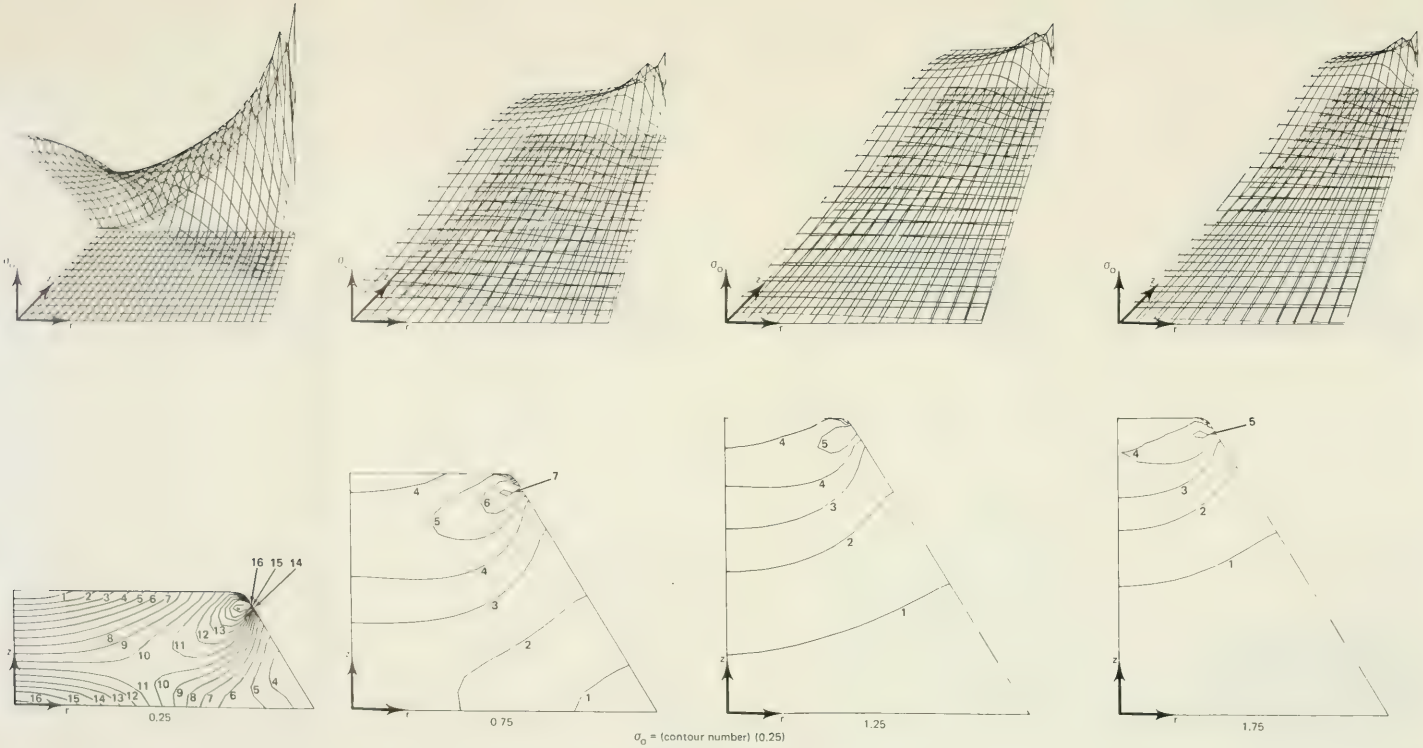


Figure 11. Effective stress contour and surface plots for 60° angle and free boundary condition.

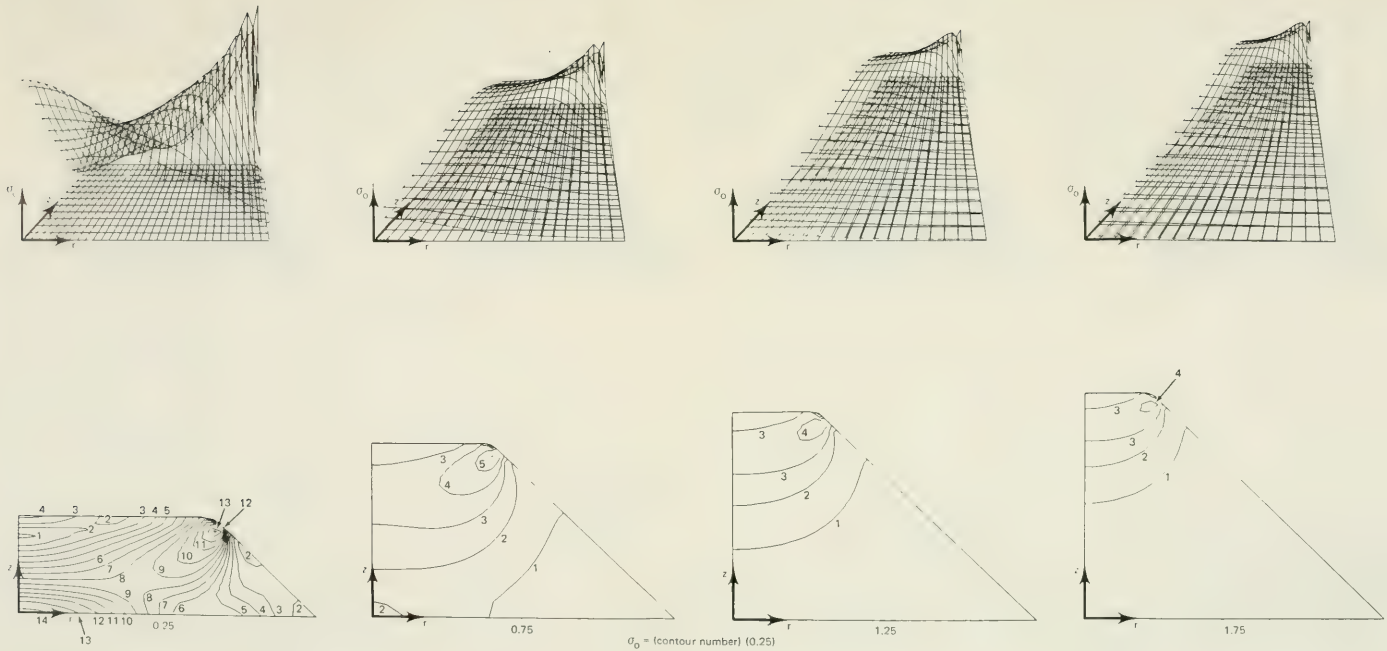


Figure 12. Effective stress contour and surface plots for 90° angle and free boundary condition.

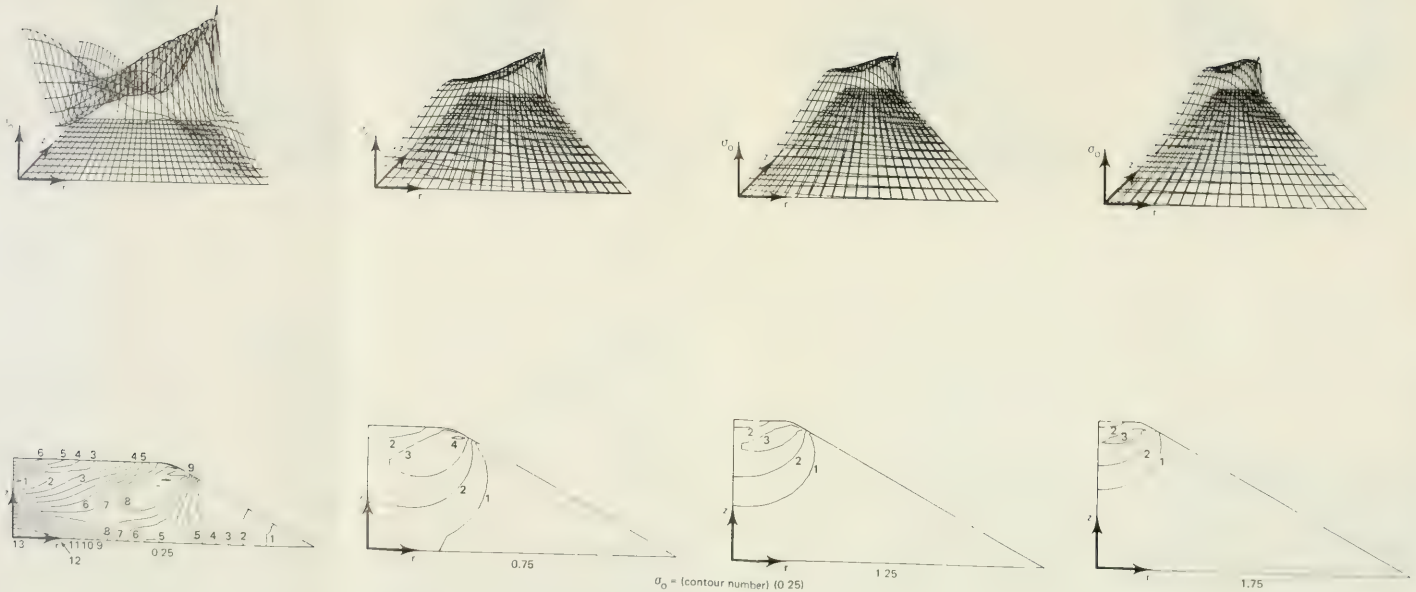


Figure 13. Effective stress contour and surface plots for 120° angle and free boundary condition.

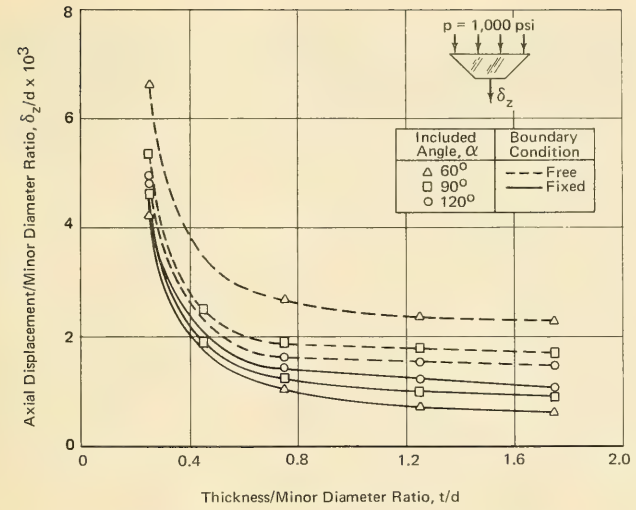


Figure 14. Instantaneous axial displacements at center of low-pressure face.

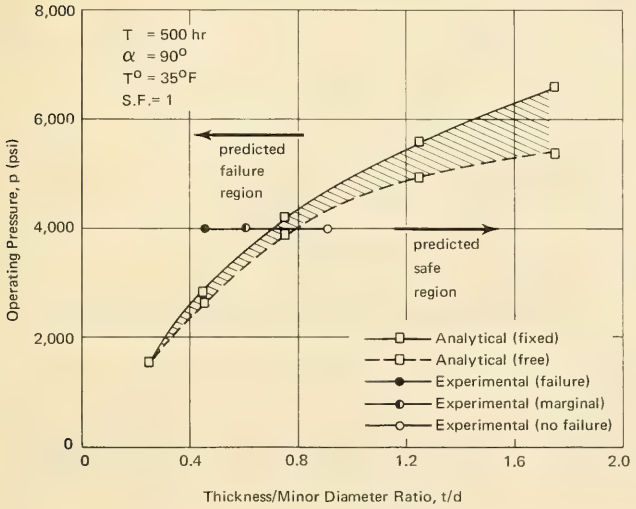


Figure 15. Comparison of experimental and analytical results.

Figure 16 compares the instantaneous displacements at the center of the low-pressure face for both the experimental and analytical work. The two analytical cases (fixed and free) successfully bracketed the experimental results. The smooth surface finish of 32 rms on the viewport flanges, in combination with the liberal use of silicone grease at the viewport-flange interface, resulted in the experimental displacements approaching the analytical free boundary condition.

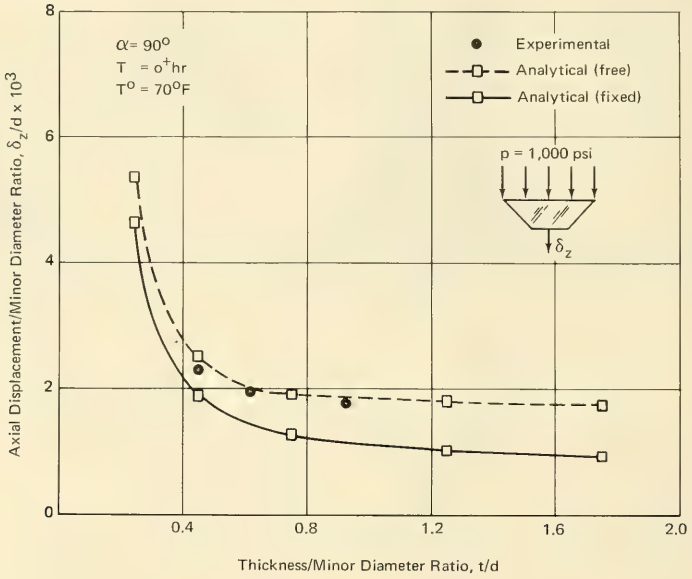


Figure 16. Comparison of experimental and analytical displacements.

## Discussion

When comparing the design curves in this report with those in Reference 2, one notices a distinct difference. The curves in Reference 2, based on ultimate strength tests, indicate an exponential increase of strength

with respect to increases in the t/d ratio. This is understandable because the strength is based solely on physically forcing the material through the flange opening. Ultimate strength tests give an indication of the catastrophic load but do not indicate at what pressure the viewport fails to fulfill its function of providing visibility.

The design curves in this report, however, are based on the visibility aspect of the viewports and show that the operating pressure or depth is limited by the yield strength of the material. As exhibited by Figures 8 through 13, the peak effective stress asymptotically approaches a finite maximum value as the t/d ratio is increased.

No extensive creep data exist at temperatures other than room temperature. One can, however, get a comparison between 35 and 70°F tests on viewports by comparing experimental displacement results of the t/d = 0.45 viewport in the main test, and the t/d = 0.45 viewport with O-ring in Appendix A. The displacement at 70°F with a time period of 500 hours was 7% greater than the displacement at 35°F for the same length of time, and after 4,800 hours the displacement was 20% greater.

Figure 17 together with Table 3 compare the analytical results of this study with the present viewport designs in operational submersibles. A load duration time of 24 hours was chosen to include the emergency time of an average vehicle. From Figure 17 it appears that many of the present designs are conservative, which was probably due to lack of structural analysis at the time of design.

## FINDINGS

Within the scope of this investigation, the following findings appear to be valid:

1. Based on both experimental and analytical results, the strength of a viewport increases with an increase in either the t/d ratio and/or the included angle for limits of 0.25 to 1.75 and 60° to 120°, respectively.

2. The maximum effective stress for a tensile region always occurs at the center of the low-pressure face with a fixed boundary condition.

3. The maximum effective stress for a compressive region always occurs at the corner of the low-pressure face with a free boundary condition.

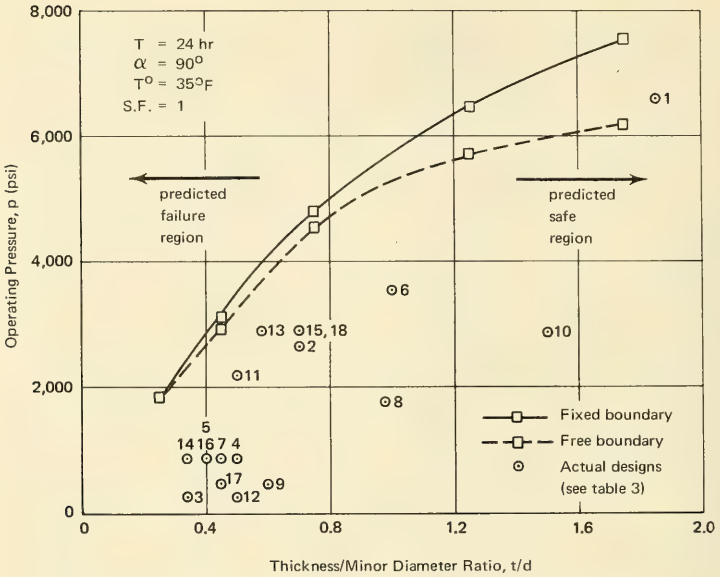


Figure 17. Comparison of analytical results and operational designs.

Table 3. Submersible Viewport Designs in Figure 17

(Extract from Reference 2.)

| Identification Number | Submersible Name | Operating Depth (ft) |
|---|---|---|
| 1 | ALUMINAUT | 15,000 |
| 2 | ALVIN | 6,000 |
| 3 | ASHERAH | 600 |
| 4 | BEN FRANKLIN | 2,000 |
| 5 | DEEP JEEP | 2,000 |
| 6 | DEEP QUEST | 8,000 |
| 7 | DEEPSTAR 2000 | 2,000 |
| 8 | DEEPSTAR 4000 | 4,000 |
| 9 | DIVING SAUCER | 1,000 |
| 10 | DOWB | 6,500 |
| 11 | DSRV | 5,000 |
| 12 | PAULO I | 600 |
| 13 | PISCES IV | 6,500 |
| 14 | ROUGHNECK | 2,000 |
| 15 | SEA CLIFF | 6,500 |
| 16 | STAR III | 2,000 |
| 17 | SURV | 1,000 |
| 18 | TURTLE | 6,500 |

4. In the actual viewport, a sharply spiked stress concentration exists at the low-pressure face corner which results in rounding of the sharp corner.

5. The transition to the dominance of flexural bending behavior occurs at about **t/d** = 0.6.

6. The stress distribution for conical frustums is independent of elastic modulus and only slightly dependent on Poisson's ratio, thus, the structural design curves are generally applicable to materials other than acrylic.

7. A conventional O-ring design with the groove located in the viewport conical face satisfactorily fulfills the requirements for viewport sealing (Appendix A).

## DESIGN RECOMMENDATIONS

The purpose of this section is to provide the designer with the necessary information to design a vehicle viewport accurately, quickly, and safely. The type of analysis used in this section was experimentally verified as previously described.

In order to design a conical acrylic vehicle viewport, the designer must have available such information as: **t/d** ratio, included angle, elevation of viewport in flange, method of sealing, and flange surface finish. The design requirements would, of course, include the operating pressure, ambient temperature, and maximum length of dive.

This section of the report deals with design curves for viewport dimensions and recommendations for elevation of viewport in flange. Design recommendations for the flange surface finish are in Reference 5, and an analysis of the viewport sealing problem is in Appendix A of this report. Annealing instructions for the viewport may be found in Appendix B or Reference 11.

### Design Curves

**Material.** Figure 18 represents the material facet of the design or the relationship between the yield stress of acrylic and time. A more detailed discussion of the origin of these curves is presented in Appendix C. The figure contains both tensile and compressive curves. The yield strengths can be seen to reduce to about 50% of the instantaneous value after 500 hours.

These curves are only for room temperature, but a temperature of $35^{o}$F will increase the yield strength by about 20% according to References 4 and 10. The strength is, of course, much lower with a higher temperature and, therefore, temperatures considerably above room temperature should be avoided.

Figure 18 is used concomitantly with Figure 19 for calculating design strength.

**Structure.** Figure 19 represents the structural facet of the design. The curves include the parameters: **t/d** ratio, included angle, safety factor, yield stress, and operating pressure. The **t/d** ratios range from 0.25 to 1.75 while the included angles range from $60^{o}$ to $120^{o}$.

The curves are based on a finite element stress analysis. With four **t/d** ratios, three included angles, and two boundary conditions (fixed and free), there were a total of 24 computer runs.

Figure 19a represents the maximum effective stress in the compression-compression-compression octant and the worst of the two boundary conditions, the free case. This point always occurred at the low-pressure face corner for the complete range of **t/d** ratios and angles. This is attributed to the plugging action creating a higher effective stress at this point.

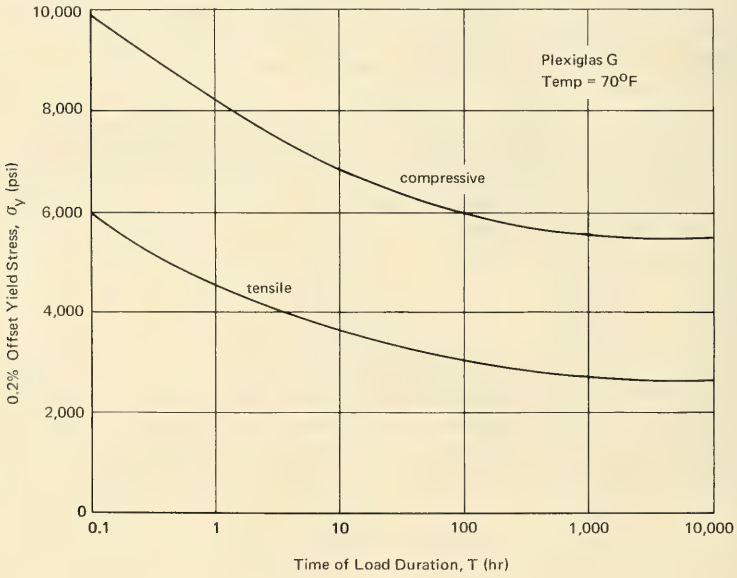


Figure 18. Yield stress-time curves for acrylic plastic.

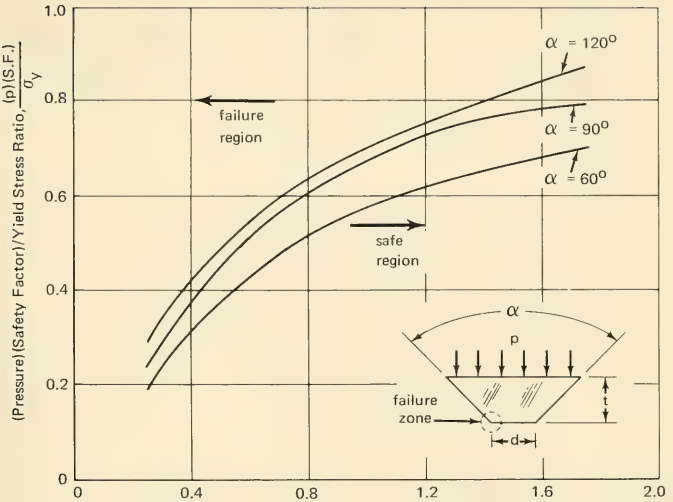


(a) Compressive region.

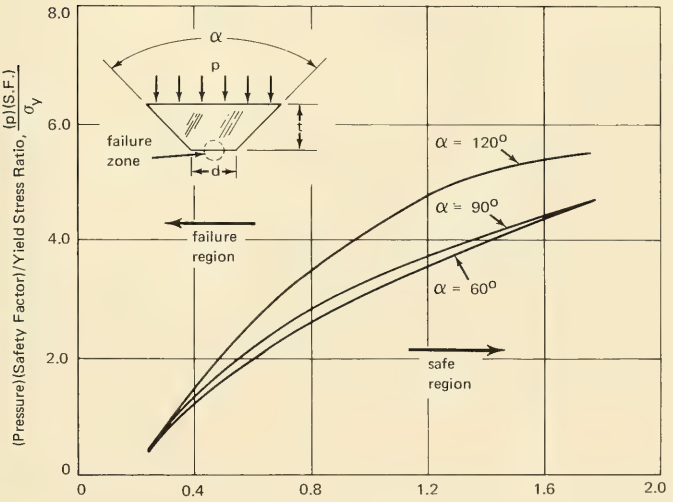


(b) Tensile region.

Figure 19. Design curves for conical acrylic viewports.

Figure 19b represents the maximum effective stress in the tension-tension quadrant due to the worst boundary condition, the fixed case. This point always occurred at the center of the low-pressure face for the complete range of the variables. The fixed boundary case was the worst due to the increase in flexural bending.

### Example

To indicate how the design curves may be used, a hypothetical case is considered. Suppose the design requirements are as follows:

Maximum operating pressure = 2,000 psi
Maximum temperature = 70°F
Safety factor = 1.5
Length of dive* = 100 hours
Included angle = 90°
Minor diameter = large as possible

To properly design this viewport, the first step is to find out what t/d ratio is necessary. From Figure 18 with an abscissa value of 100 hours, the following results are obtained:

compressive yield stress = 6,000
tensile yield stress = 3,000

Proceeding to Figures 19a and 19b, and calculating the ordinate value for each curve

compressive $\frac{(p)\ (S.F.)}{\sigma_y} = \frac{(2{,}000)\ (1.5)}{6{,}000} = 0.5$

tensile $\frac{(p)\ (S.F.)}{\sigma_y} = \frac{(2{,}000)\ (1.5)}{3{,}000} = 1.0$

Using the above ordinate values, the following t/d ratios were taken off the abscissa:

from Figure 19a t/d = 0.58
from Figure 19b t/d = 0.34

---

* This assumes that there is adequate relaxation time between dives.

To safely withstand the operating requirements, a t/d ratio of 0.58 or larger would be used. Since the minor diameter is to be as large as possible and commercial acrylic sheets come in thicknesses up to 4 inches

$$t/d = 0.58$$

$$\therefore d = \frac{t}{0.58} = \frac{4}{0.58} = 6.9 \text{ inches}$$

The largest minor diameter would be 6.9 inches.

The elevation, h, (see Figure 2) of the viewport in the flange is another important aspect of the total viewport design. Using a t/d ratio of 0.58 on the abscissa of Figure 14, a value for the ordinate is obtained

from Figure 14 (free boundary) $\quad \frac{\delta_z}{d} = 0.0021$ inch per 1,000 psi

It is recommended by the authors that the viewport be elevated five times the analytical (free case) displacement

$$h = 5\delta_z = (5)\left(\frac{0.0021}{1{,}000}\right)(6.9)(2{,}000) = 0.145 \text{ inch}$$

For safe operation of the viewport, a minimum elevation of 0.15 inch should be used in this particular design to insure adequate distance to the end of the conical surface, again recognizing the fact that any significant elevation above this achieves nothing (stress distribution remains the same) and, in fact, only adds additional flange material (i.e., weight) to the vehicle.

Figure 19 provides for the use of a safety factor in designing conical viewports. Safety factors are utilized when a designer cannot control all of the many extraneous variables during fabrication and service that might affect his original design. In view of the in-depth research for both the structure and the material properties contained in this report, and the reproducibility of commercial Plexiglas, the authors feel that a safety factor of 1.5 is more than adequate, if all other design recommendations contained herein are followed.

## ACKNOWLEDGMENT

Mr. John McKay conducted the experimental tests and reduced the experimental data used in this study.

## Appendix A

## INVESTIGATION OF A VIEWPORT SEAL DESIGN

### INTRODUCTION

A necessary, although oftentimes neglected, function of a viewport design is that of maintaining waterproof integrity at all times. Even very small leaks would be detrimental in a habitat (long term submergence) because of the large accumulation over a long length of time, not to mention the psychological effects on the occupants. Waterproof integrity is accomplished by a viewport seal system which must function in two environments: (1) at the surface both before and after dives (low pressure), and (2) at the operating depth (high pressure).

The objective of this appendix is to (1) review and evaluate existing methods of sealing submersible (short term submergence) viewports, but with regard to the additional habitat functional requirements, and (2) investigate both experimentally and analytically the most promising of the designs.

### BACKGROUND

To provide waterproof integrity, the first viewport seal designs relied on a lapped-joint seal between the viewport and flange as shown in Figure A-1a. Achievement of the seal is by 80 to 90% contact surface area, which requires surface finishes in the 8 to 32 rms range. This design maintained a seal at the lapped joint for both low-pressure and high-pressure sealing. Sometimes a flat gasket is used for padding between the retainer ring and viewport.

The next design was the gasket seal as shown in Figure A-1b. This particular design relied on a gasket located at the perimeter of the high-pressure face for low-pressure sealing and on the lapped joint for high-pressure sealing.

A similar design, as shown in Figure A-1c, had an O-ring located at the corner of the viewport high-pressure face. Here again the low-pressure sealing was accomplished by the O-ring and the high-pressure sealing by the lapped joint.

The design shown in Figure A-1d is currently being used for submersibles. Here both high-pressure and low-pressure sealing is accomplished by the O-ring seal.

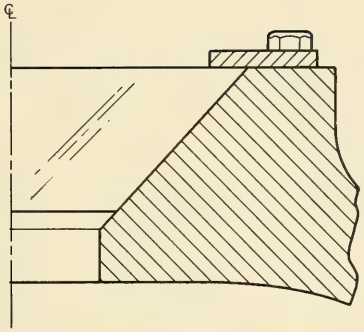

(a) Lapped-joint seal.

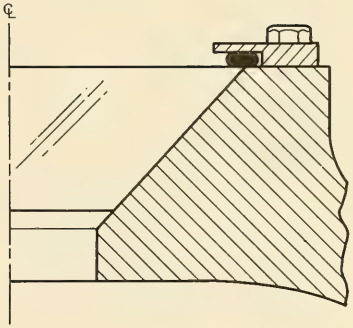

(b) Gasket seal.

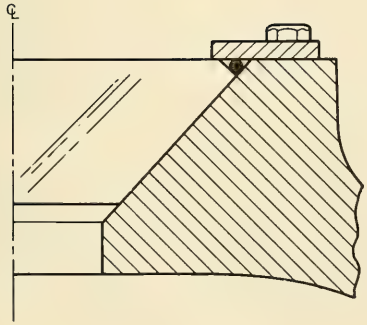

(c) O-ring seal no. 1.

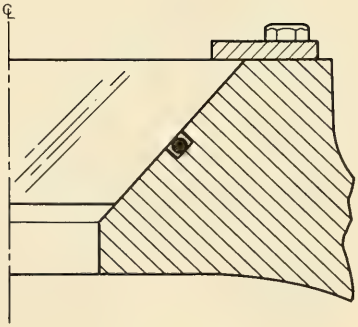

(d) O-ring seal no. 2.

Figure A-1. Current viewport seal designs.

Submersible designs are not necessarily acceptable for habitat designs because of the more stringent functional requirement due to creep. It would, therefore, be worthwhile investigating a new seal design which would meet the requirements and still reduce cost without compromising the structural integrity of the viewport. A new design or variation of the seal in Figure A-1d is shown in Figure A-2. It is a conventional circular O-ring in a rectangular groove located on the conical face of the viewport. Note that all five designs discussed require retainer rings.

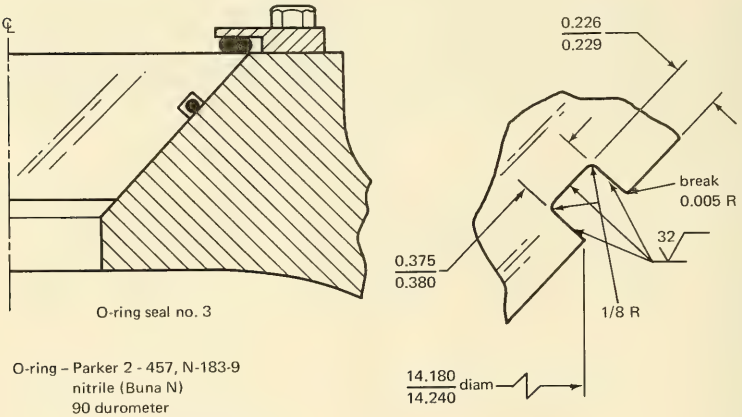


Figure A-2. Recommended viewport seal design.

## COMPARISON OF DESIGNS

The five seal designs described may be compared in three different areas: (1) operation, (2) economy, and (3) structure.

### Operation

Functional requirements for viewport seal systems include sealing under all conditions. As previously observed in the main body of this report, creep occurs in the viewport after a long term submergence. Even after returning to the surface, the viewport does not immediately return to its

original position. Therefore, the first three seal designs, a, b, and c, in Figure A-1, would find it difficult to efficiently seal after the habitat surfaces. Neither the retainer ring, gasket, nor O-ring seal no. 1, respectively, would be able to follow the creep displacement of the viewport; the necessary compression of the components for sealing would be lost. These designs function perfectly for submersibles because their dive times are short, thus minimizing the effects of creep.

O-ring seal no. 2 and O-ring seal no. 3 are both able to follow the displacement of the viewport and to maintain the seal. A compressible gasket might be employed at the retainer ring-viewport interface, not as a seal, but as a spring to maintain pressure on the viewport for low-pressure sealing. Operationally, an O-ring that is stretched around the viewport (O-ring seal no. 3) is much easier to work with than the reverse (O-ring seal no. 2). The design in Figure A-2 appears to exhibit operational advantages over the other four designs.

The success of such a seal system (Figure A-2) has already been proven under long term tests in the ocean. Jenkins and Reinhart[12] tested such a design, a conventional O-ring seal in an angular flange, for 189 days at a depth of 5,900 feet in the Pacific Ocean. The O-ring gland materials were carbon steel, aluminum, and clad steel. The O-ring material was nitrile (Buna N) with a hardness of 90 Shore A durometer. The lubrication was petroleum based, although a silicone grease is recommended to preclude any deleterious effect on the acrylic. Results of the tests indicated: (1) no deterioration of the O-ring material, (2) no significant change in O-ring hardness or resilience, (3) no significant amount of water absorption by the O-ring, and (4) no leakage past the seal system.

### Economy

The total cost of a viewport assembly could be reduced if an O-ring seal was used rather than a lapped-joint seal. Lapped-joint seals are extremely expensive due to: (1) manual lapping of viewport, (2) tight tolerances on dimensions, (3) additional machining for smooth surface finishes, and (4) absence of interchangeability of viewports. Even for low-pressure sealing, seal systems a, b, and c in Figure A-1 require tight tolerances to insure that the viewport seats at the correct level in the flange.

O-ring seals no. 2 and no. 3 on the other hand, can seal anywhere on the faying surfaces so the tolerances need not be so tight. Between the two designs, no. 2 and no. 3, the latter appears to be the more economical. In initial fabrication, it would be more economical to cut the groove in the easily machined acrylic. Also, if the flange is to be clad for corrosion purposes, the process is more economical if it is not necessary to contend with

an O-ring groove. Since the flange is usually welded to the steel pressure hull, it would be cheaper to replace a damaged O-ring groove in the viewport as opposed to a damaged one in the flange.

### Structure

With the design in Figure A-2 exhibiting advantages both operationally and economically, it remains only a question of whether the viewport can structurally withstand the stress concentration due to the presence of the O-ring groove. The earlier seal designs in Figure A-1 did not structurally affect the viewport. Designers probably did not use the design in Figure A-2 because of the unknown effects of the stress concentration; there was no thorough stress analysis until Reference 5 was completed.

The possibility does exist with O-ring seal no. 2 in Figure A-1, that the softer acrylic will creep down into the O-ring groove in the flange and cause an extremely high stress concentration that could be catastrophic with long term loading.

The O-ring groove in the viewport seal design of Figure A-2 was located near the high-pressure face because the results discussed in the main text of this report indicated that the stress distribution was nearly hydrostatic in this area. The rest of this appendix is concerned only with the design in Figure A-2 and the structural response of the viewport to the presence of the O-ring groove.

## SCOPE OF INVESTIGATION

To thoroughly determine the structural effect of the groove on the viewport, both an experimental and analytical phase were conducted on the design shown in Figure A-2.

### Experimental Phase

The viewport used to test the O-ring design was very similar to the $t/d = 0.45$ viewports used in the main text and is shown in Figure A-3. The temperature during the test was maintained between 65 and 75$^{o}$F because this would impose a more severe test than a lower temperature. While the pressure was held at 4,000 psi, the displacements at the center of the low-pressure face were recorded until the displacements became asymptotic within the measurement accuracy. The machining procedure, pressure vessel type, and testing procedures are all discussed in Appendix B.

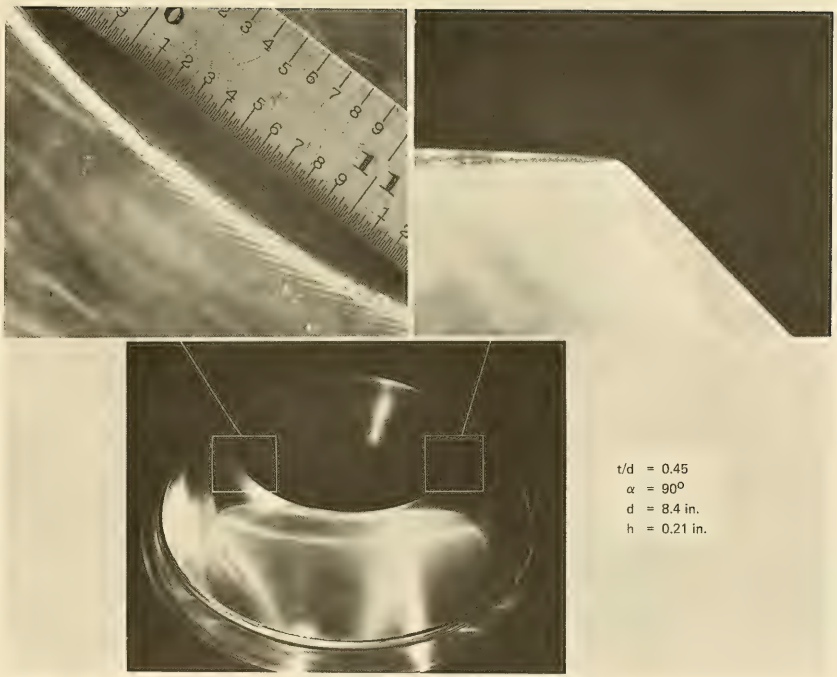


Figure A-3. Post-test physical condition of t/d = 0.45 viewport with O-ring after 200 days.

### Analytical Phase

The viewport was simulated using the finite element method to obtain effective stress values at critical points for later analysis. The mesh contained 664 nodal points and 610 elements. Both the free and fixed boundary conditions were used in this analysis.

## RESULTS

### Experimental

The viewport with the O-ring was loaded at 4,000 psi for a total time of 200 days before the creep leveled off. Post-test observations, as shown in Figure A-3, indicated rounding of the corner and presence of cracks. Inspection of the O-ring groove, however, found no crazing or cracks whatsoever. Figure A-4 presents the absolute displacement at the center of the low-pressure face versus time in days. Creep accounted for 35% of the total displacement at 200 days. Even with this much displacement the O-ring did seal when the dive was completed and the viewport was relaxing.

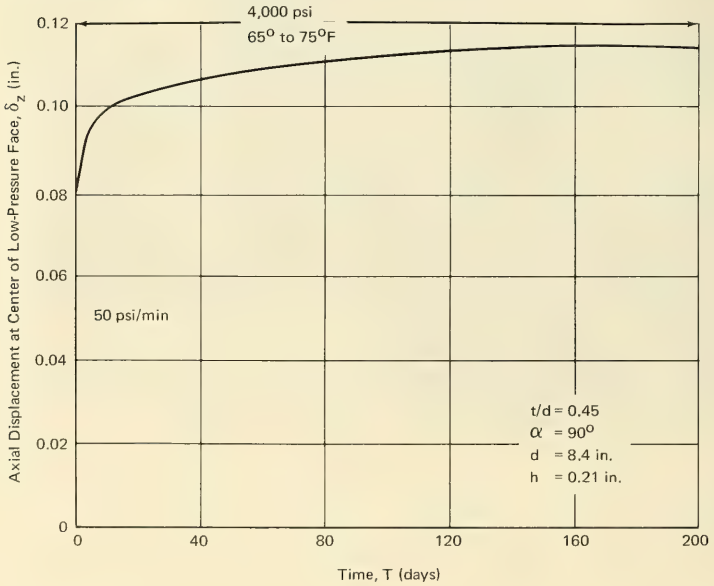


Figure A-4. Displacement response of viewport with recommended seal design.

## Analytical

Figure A-5 shows the resulting contour plot of effective stresses for the viewport with the O-ring. Two stress concentrations are clearly found: (1) at the low-pressure face corner, and (2) at the O-ring groove. Table A-1 summarizes the data at the critical locations and indicates that the maximum effective stress value around the O-ring groove is only about one-half that at the low-pressure face corner. The boundary condition essentially created no difference in the stresses around the O-ring groove.

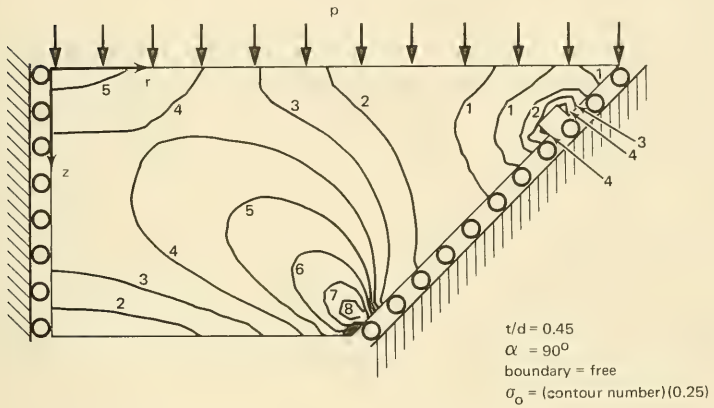


Figure A-5. Effective stress contour plot for 90° angle and free boundary condition with O-ring groove.

Table A-1. Effective Stress, $\sigma_o$, for Viewport With O-Ring Groove

| Location | Boundary Condition | |
|---|---|---|
| | Fixed | Free |
| Maximum at O-ring groove (compressive) | 1.15 | 1.41 |
| Center of low-pressure face (max tension) | 0.728 | no tensile stresses |
| Low-pressure face corner (max compressive) | 2.51 | 2.58 |

## DISCUSSION

The experimental results and the analytical results had excellent agreement. Even when the viewport failed at the low-pressure face corner, there was no failure at the O-ring groove. The design recommendations (Figures 18 and 19a) of this report predicted failure for this viewport and, as shown in Figure A-3, failure occurred.

It might also be interesting to note the flexural behavior of this viewport as shown in Table A-1. For the free boundary condition, no tensile stresses appeared at the center of the low-pressure face as they did for the fixed boundary case.

Although minimum research time negated any investigation of mesh-size influence on the O-ring groove, the results were in agreement with the experimental results. Also, the analytical simulation of the groove was a worst case solution. This means there was no rounding of the corners in the simulated model while in the experimental case the corners had a 1/8-inch radius.

## FINDING

A conventional O-ring design with the groove located in the conical face of the viewport (Figure A-2) satisfactorily fulfills the requirements for viewport sealing in three ways: operationally, economically, and structurally.

Appendix B

# EQUIPMENT AND PROCEDURE FOR EXPERIMENTAL PHASE

## INTRODUCTION

Information relative to the design and operation of equipment for the simulated operational tests on full-scale viewports is contained in this appendix. The testing requirements were as follows:

1. Test at least three sizes of full-scale viewports
2. Pressure range, 0 to 4,000 psi
3. Temperature range, $35^{\circ}$ to $70^{\circ}$F
4. Test time, 1 year
5. Cycling to simulate dives of an undersea vehicle

Due to the size of the viewports and the length of time of the tests, a decision was made to design pressure vessels and a refrigeration system specifically for these tests. As a result, pressure vessels with other capabilities would not be tied up for a year.

## HIGH PRESSURE SYSTEM

### Pressure Vessels

The pressure vessel design was as shown in Figure B-1. This particular design yielded the following advantages:

1. Efficiency—each vessel tested two viewports at one time.
2. Safety—low volume of fluid to negate "bomb" danger.
3. Economy—materials and fabrication costs were low.
4. Ease of operation—simplicity and compactness of design allows ease in pressure and temperature cycling.
5. True simulation—low-pressure face exposed to constant room temperature while high-pressure face exposed to simulated cycling of temperature and pressure.

There were two possible disadvantages to the design: (1) opening and closing of a vessel was time consuming and (2) the O-ring extruded when operated to any reasonable pressure and required replacement after each test. These disadvantages are not severe because the system is for long term operation, not day-to-day operation. A typical pressure vessel consisted of two 32-inch-diameter steel flanges as shown in Figure B-1. The conical surfaces of the flanges were machined to a 32 rms finish. The three vessels had through-hole nominal diameters of 4, 6, and 8 inches.

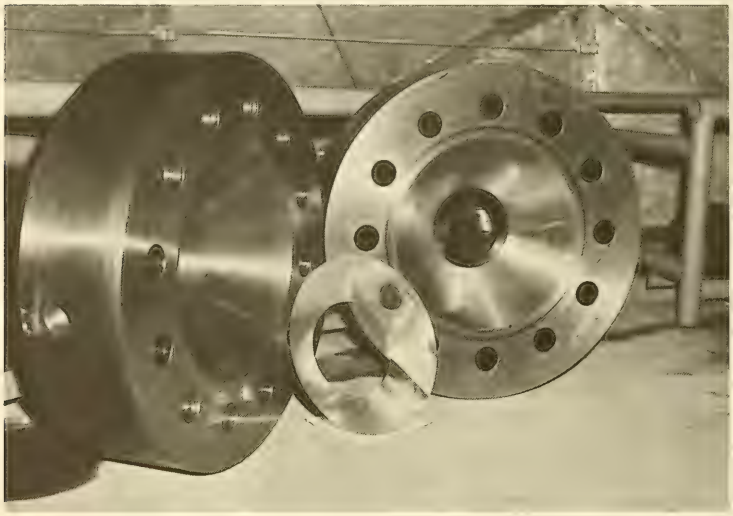

**Figure B-1. Typical pressure vessel flanges with an 8-inch minor diameter viewport.**

### High-Pressure Pump

The high-pressure pump was an air-driven double-acting piston type rated for 20,000 psi. Tubing made of 1/4-inch-diameter, 316 stainless steel connected the pump to the accumulator.

### Accumulator

The air/water accumulator provided a means of storing energy in the high-pressure system to maintain a constant pressure in the vessels. The vessels were all connected to a common manifold, thus, pressure cycling was identical for all three vessels.

## REFRIGERATION SYSTEM

A refrigeration system was necessary in this study to aid in simulating actual environmental conditions. Located on the pressure vessels were Plate-Coil heat transfer units as shown in Figure B-2a. The single, embossed units were rolled to the vessel diameter to insure adequate heat transfer between the vessels and the units. Two units which were connected together by a jumper hose were necessary for one vessel. A heat transfer cement, Thermon T-3, was used between the vessel and heat transfer units to increase the overall heat transfer coefficient. Sheets of an elastomeric insulation, Armaflex, were used on top of the heat transfer units as shown in Figure B-2b. Glycol brine was circulated through the refrigeration system. Cooling was provided by a 5-ton-capacity air-cooled chiller. Temperature measurements were taken at both the inlet and outlet of the chiller.

## INSTRUMENTATION SYSTEM

Dial indicators, as shown in Figure B-3, were utilized on each of the six viewport faces to measure absolute displacement of the center of the face with respect to the pressure vessel. Lufkin dial indicators with graduations of 0.001 inch were used. The averages of the displacement readings for the three pairs of viewports in the pressure vessels were calculated and are presented in Figure 7 of this report.

Pressure gages with a range of 5,000 psi were the high-pressure measuring system, while a 50-psi gage was used on the no-load part of the cycle. Here it was necessary to maintain a 1 to 5-psi load to keep the viewport in position.

## VIEWPORTS

The seven viewports in this study (including one used in the O-ring test) were machined from a 4-foot by 5-foot by 4-inch cast sheet of Plexiglas G acrylic plastic. The viewports were rough machined and then annealed in accordance with the manufacturer's recommendations[11] as follows:

| Section Thickness (in.) | Annealing Temp ($^{o}$F) | Time (hr) | Cooling Rate ($^{o}$F/hr) |
|---|---|---|---|
| 4 | 175 | 22 | 5 |

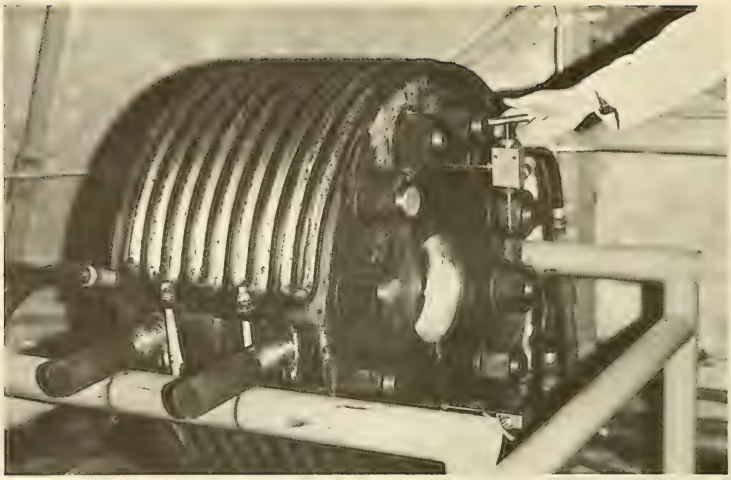

(a) Heat transfer units installed on pressure vessel.

(b) Pressure vessel with installed insulation.

Figure B-2. Typical pressure vessel with refrigeration system.

Upon completion of initial anneal, the viewports were machined to final dimensions and annealed again. The viewports were polished to an optical finish before testing to facilitate post-test observations of possible cracks.

Figure B-3. Experimental test setup.

All minor diameters of the viewports were designed larger than the penetrations in the pressure vessel to elevate the viewport in its seat in order to avoid the stress concentration at the break of the conical surface.

Because the test occurred over such a length of time, it was necessary to insure accuracy of results. Therefore, two viewports of the same dimensions were tested at the same time to provide redundancy to the test.

## TEST PROCEDURE

The conical surfaces of the viewports were first coated with Dow Corning No. 4 silicone grease, a lubricant which will not attack the acrylic plastic. After the six viewports were placed in the three vessels, the vessels were filled with tap water. Initially, the pressure was raised to 2,000 psi and quickly returned to 0 psi. This procedure seated the viewports, squeezed out a majority of the excess grease, and allowed the dial indicators to be zeroed. Subsequently, the pressure and temperature were changed simultaneously

from 0 to 4,000 psi and 70 to 35°F, respectively. This portion of the cycle represented the dive of the vehicle. Upon completing the desired loading time of 500 hours, the pressure and temperature were simultaneously changed from 4,000 to 0 psi and 35 to 70°F, respectively.

The displacements at the center of the low-pressure face were taken twice a day except for weekends and holidays. The morning and the afternoon were chosen for the displacement recordings because the minimum and maximum pressures for each working day corresponded with the minimum and maximum temperature fluctuations for the 24 hours of the day.

Appendix C

# FAILURE CRITERION APPLIED TO CONICAL ACRYLIC VIEWPORTS

## A FAILURE CRITERION

This appendix outlines the development of a rational yield-failure theory utilized in the design guidelines of this report.

In keeping with the yield-failure definition set forth in this report, two entities must be completely described. First, the location and relative magnitude of the maximum effective stress, $\sigma_o$, must be evaluated; and second, the material yield strength, $\sigma_y$, must be determined. Unfortunately, acrylic exhibits time dependency, consequently, both of the above entities are functions of time, i.e., loading history. Because of the infinite variety of possible loading histories, the general design procedure would be to choose the most unfavorable loading history to account for all other less severe cases.

For the special case of acrylic viewports, the most detrimental loading history would be represented by a step loading raised immediately to maximum operational depth and held there for the given duration. Moreover, if acrylic was purely viscoelastic, the stress distribution in the viewport at time $T = 0^+$, is identical to the distribution resulting from an elastic analysis and represents the most unfavorable distribution in terms of the high magnitudes and stress concentrations. As time progresses, stress relaxation occurs relieving and redistributing high stress concentrations. Thus, in terms of the viscoelastic behavior, the elastic solution $(T = 0^+)$ may be conservatively used to determine the maximum stress concentrations and assume these magnitudes constant with time rather than decreasing. Actually, the conservative assumption of constant viewport stresses is quite accurate due to the phenomenon that the elastic stresses of conical frustums are independent of Young's modulus and only slightly dependent on Poisson's ratio. Hence, in view of the correspondence principle, which relates elastic and viscoelastic solutions, time would have very little effect on the viscoelastic stresses. In light of the above, one can rationally accept the stresses resulting from an elastic analysis (approximated by the finite element technique) as the governing stresses throughout the loading duration, providing there is adequate recovery time between loadings.

The effect of time on the material yield stress, $\sigma_y$, which has been observed to decrease as loading time progresses, is next considered. A graphical relationship of this is presented in Figure 18 in the Design Recommendation portion of this report. At this point, a qualitative outline is presented, illustrating the origination of the graph.

Consider the typical creep data shown in a of Figure C-1 where each curve represents the strain-time relation for a given level of stress. If a particular time, $T_1$, is selected and corresponding values of stress and strain are plotted as shown in b of Figure C-1, an isochronous stress-strain relationship results. Because time has been held constant, any curvature in the stress-strain relation is due to either yielding or nonlinearity of the material. Curvature arising solely from nonlinearity does not limit the yield-strength of the material as previously defined, however, existing creep data for acrylic does not contain unloading histories and permanent set records, thus rendering it impossible to separate the effect of nonlinearity from yielding. Therefore, it was conservatively assumed that all curvature was due to yielding and that the yield strength at time $T_1$ was defined as the 0.2% offset strain intersect of the isochronous stress-strain relation. Following the above procedure for several different times of interest, a curve can be generated as in c of Figure C-1 which establishes the yield-stress versus load-time relationship. The graph of this relationship for acrylic, displayed in Figure 18, was derived from creep data obtained from three sources.[10,13,14] For some loading durations, creep data were nonexistent for Plexiglas G, but were approximated by engineering judgments of creep data on Plexiglas I-A.

## A STRESS SINGULARITY AND THE ANALYTICAL TOOL (FINITE ELEMENT)

In modeling the viewport by the finite element technique, a preliminary investigation was conducted to determine an adequate number of quadrilateral elements to represent the system. It can be shown by variational theorems that the finite element solution approaches the exact solution as the number of elements approach infinity. Of practical importance, the convergence of the finite element model can be determined by comparing stresses obtained from a coarse mesh with those obtained from a finer mesh. In so doing, it was discovered that about 400 elements was a sufficient number, such that, further increase in the number of elements did not appreciably alter the numerical values of stresses at a given point. This held true throughout the entire cross section except for one very notable

point, namely, a minute region in the neighborhood of the low-pressure face corner. At this particular location all stresses were becoming exceedingly higher as the number of elements were increased. Further subdivision in this corner revealed that these stresses were becoming arbitrarily high, suggesting that the corner point stresses would approach infinitely high values if the subdividing process continued. In witness of this phenomenon, Figure C-2 portrays the computed effective stress as a surface over the cross section of a typical viewport in which the corner has been finely subdivided. This representation readily depicts the singular nature of this stress concentration as a Dirac spike. It was hypothesized that this spike has physical significance and that it is not simply an error emanating from the numerical technique involved. In support of this contention, it was observed that all experimental viewports exhibited a minute permanent plastic deformation at this corner even for moderate loads.

Taking the cue from experimental observations, the corner of the analytical model was "rounded" in an attempt to model the plastic deformation occurring in the actual viewport. Furthermore, care was taken to determine what effect various amounts of "rounding" had on the resulting stresses. It was discovered that the percentage of area removed did not alter stress values significantly providing the percentage of deformation (percentage of area removed) was greater than about 0.02%. Figure C-3 illustrates this relationship where it is seen that the relative maximum effective stress stabilizes for deformation percentages above 0.02%, ***independent of the mesh size***. In view of this, it was hypothesized that in a physical case the viewport would deform approximately 0.02% to relieve the Dirac spike stress concentration. This contention was supported by the percentage of deformation measured in the viewport shown in Figure 4 of this report.

In summary, the philosophy to be adopted in comparing the analytical and experimental results is that, under initial loading, the actual viewport will undergo minute local yielding which results in deformation at the low-pressure face corner, to relieve itself of the spiked stress concentration. This results in a "modified" structure which, when analyzed, does not display the Dirac spike stress concentration, but rather a realistic stress concentration with some finite value. Thus, from the analytical standpoint, the initial yielding problem is dismissed by beginning the analysis with the modified structure (deformed corner). Accordingly, the failure definition applies to the modified structure for both fixed and free boundary condition.

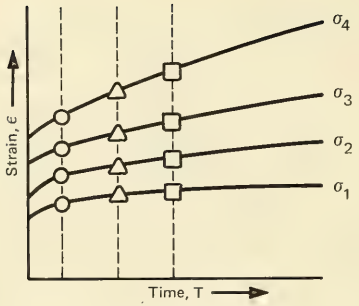


(a) Creep curves.

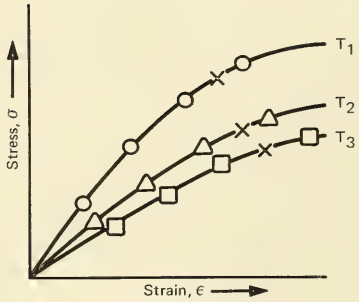


(b) Isochronous curves.

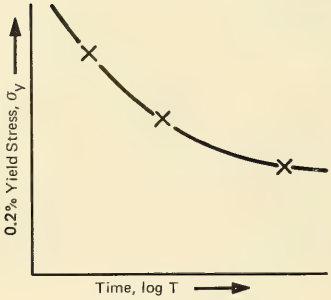


(c) Yield stress-time curve.

Figure C-1. Material property curves for acrylic plastic.

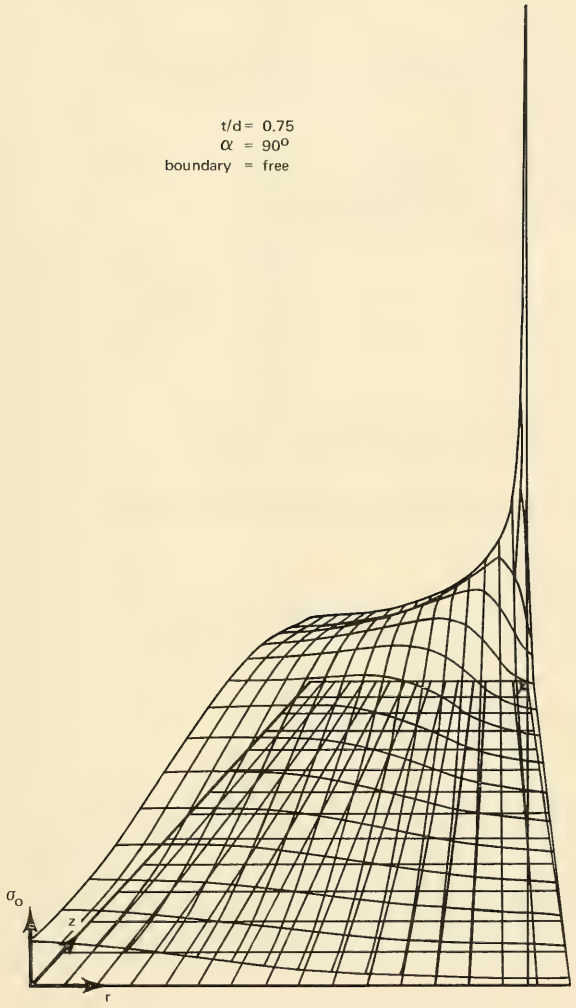


Figure C-2. Effective stress surface plot for sharp corner.

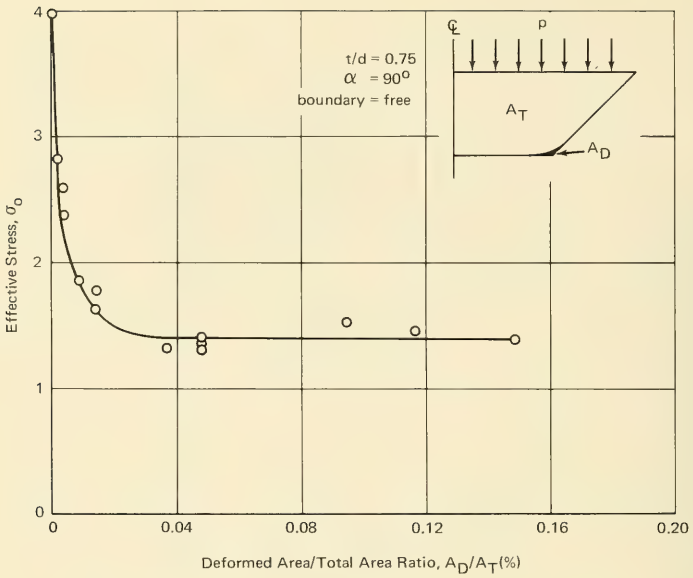


Figure C-3. Effective stress variation at low-pressure face corner.

## REFERENCES


1. A. Piccard. Earth, sky and sea. New York, Oxford University Press, 1956.

2. M. R. Snoey and J. D. Stachiw. "Windows and transparent hulls for man in hydrospace," in A critical look at marine technology; transactions of the 4th annual MTS conference & exhibit, Washington, D.C., July 8-10, 1968. Washington, D.C., Marine Technology Society, 1968, pp. 419-463.

3. Allied Research Associates, Inc. Technical Report ARA 350-3: Tests of acrylic deep submergence windows under simulated operational conditions, by R. Winter and J. Pozerycki. Concord, Mass., Sept. 1968. (Contract no. N00024-67-C-5351) (AD 848287)

4. Naval Ship Research and Development Center. Technical Report 2944: Evaluation of full-scale DSRV-1 acrylic windows under external pressure, by M. A. Krenzke, M. C. Breiter, and L. N. Gifford. Washington, D.C., Jan. 1969. (AD 849354)

5. Naval Civil Engineering Laboratory. Technical Report R-675: Stress analysis of a conical acrylic viewport, by M. R. Snoey and J. E. Crawford. Port Hueneme, Calif., Apr. 1970.

6. A. Nadai. Theory of flow and fracture of solids, vol. 1. New York, McGraw-Hill, 1950.

7. General Electric Company. Advanced Technology Laboratories. Report No. 61GL181: The effects of biaxial stresses on the deformation and fracture of polymethylmethacrylate, by R. L. Thorkildsen and W. V. Olszewski, Schenectady, N.Y., Apr. 1962.

8. Army Missile Command. Physical Sciences Laboratory. Report No. RR-TR-64-15: Combined stress properties for acrylic tube specimens, by R. E. Ely. Redstone Arsenal, Ala., Aug. 1964. (AD 450662)

9. E. L. Wilson. "Structural analysis of axisymmetric solids," American Institute of Aeronautics and Astronautics, Journal, vol. 3, no. 12, Dec. 1965, pp. 2269-2274.

10. Armed Forces Supply Support Center. Military Handbook MIL-HDBK-17: Plastics for flight vehicles, pt. 2. Transparent glazing materials. Washington, D.C., Aug. 1961.

11. Rohm and Haas Company. Publication no. PL-28n: PLEXIGLAS design and fabrication data, Rev. ed. Philadelphia, Pa., Sept. 1964.

12. Naval Civil Engineering Laboratory. Technical Note N-1072: Seal systems in hydrospace, Phase III: Effects of long-term hydrospace exposure on seal system integrity. 189 days at 5900 feet, by J. F. Jenkins and F. M. Reinhart. Port Hueneme, Calif., Jan. 1970.

13. J. Marin and Y. Pao. "On the accuracy of extrapolated creep-test relations for plexiglas subjected to various stresses," American Society of Mechanical Engineers, Transactions, vol. 74, Oct. 1952, pp. 1231-1240.

14. Rohm and Haas Company. PLEXIGLAS handbook for aircraft engineers, 2nd ed. Philadelphia, Pa., 1952, pp. 15-16.

## LIST OF SYMBOLS

| | |
|---|---|
| $A_D$, $A_T$ | Deformed and total areas of viewports, $in.^2$ |
| D | Diameter of high-pressure face, in. |
| d | Diameter of low-pressure face, in. |
| h | Elevation of viewport in flange, in. |
| p | Pressure applied to viewport, psi |
| r | Radial coordinate, in. |
| S.F. | Safety factor |
| T | Time, indicated units |
| $T^o$ | Temperature, $^oF$ |
| t | Thickness of viewport, in. |
| z | Axial coordinate, in. |
| $\alpha$ | Included angle of conical viewport, degrees |
| $\delta_z$ | Axial displacement of viewport, in. |
| $\epsilon$ | Strain, in./in. |
| $\theta$ | Tangential coordinate, degrees |
| $\sigma_1,\sigma_2,\sigma_3$ | Principal stresses per unit of applied pressure, psi/psi |
| $\sigma_o$ | Effective stress per unit of applied pressure, psi/psi |
| $\sigma_y$ | Yield stress, psi |

## DISTRIBUTION LIST

| SNDL Code | No. of Activities | Total Copies | |
|---|---|---|---|
| — | 1 | 20 | Defense Documentation Center |
| FKAIC | 1 | 10 | Naval Facilities Engineering Command |
| FKNI | 10 | 10 | NAVFAC Engineering Field Divisions |
| FKN5 | 9 | 9 | Public Works Centers |
| FA25 | 1 | 1 | Public Work Center |
| — | 11 | 11 | RDT&E Liaison Officers at NAVFAC Engineering Field Divisions and Construction Battalion Centers |
| — | 310 | 310 | NCEL Special Distribution List No. 9 for persons and activities interested in reports on Deep Ocean Studies |

Naval Civil Engineering Laboratory
STRUCTURAL DESIGN OF CONICAL ACRYLIC VIEWPORTS
(Final), by M. R. Snoey and M. G. Katona
TR-686 57 p. illus June 1970 Unclassified

1. Acrylic plastic viewports 2. Conical shape I. YF 38.535.005.01.005

The purpose of this report is to establish a rational engineering approach for the design of conical acrylic viewports. To achieve this goal, a time-dependent, yield-failure criterion was developed and utilized in the analysis of a variety of viewport configurations. Specifically, a range of thickness/minor diameter (t/d) ratios from 0.25 to 1.75 and included angles from 60° to 120° were analyzed by the finite element technique. Using the viewport structural analysis in conjunction with the yield-failure criterion for acrylic, time-dependent operating depths were determined as a function of viewport configuration. Paralleling the above, an experimental investigation was performed to validate the analytical results. Six full-scale viewports were tested for a year under simulated operational conditions that included simultaneous cycling of pressure and temperature, 0 to 4,000 psi and 70 to 35°F, respectively. Design recommendations are presented in the form of design curves which enable the design of a conical acrylic viewport for a specified operating pressure and duration under load. To complete the recommendations, design information is given also on sealing with a conventional O-ring, as well as guidelines for elevating a viewport in its flange.

Naval Civil Engineering Laboratory
STRUCTURAL DESIGN OF CONICAL ACRYLIC VIEWPORTS
(Final), by M. R. Snoey and M. G. Katona
TR-686 57 p. illus June 1970 Unclassified

1. Acrylic plastic viewports 2. Conical shape I. YF 38.535.005.01.005

The purpose of this report is to establish a rational engineering approach for the design of conical acrylic viewports. To achieve this goal, a time-dependent, yield-failure criterion was developed and utilized in the analysis of a variety of viewport configurations. Specifically, a range of thickness/minor diameter (t/d) ratios from 0.25 to 1.75 and included angles from 60° to 120° were analyzed by the finite element technique. Using the viewport structural analysis in conjunction with the yield-failure criterion for acrylic, time-dependent operating depths were determined as a function of viewport configuration. Paralleling the above, an experimental investigation was performed to validate the analytical results. Six full-scale viewports were tested for a year under simulated operational conditions that included simultaneous cycling of pressure and temperature, 0 to 4,000 psi and 70 to 35°F, respectively. Design recommendations are presented in the form of design curves which enable the design of a conical acrylic viewport for a specified operating pressure and duration under load. To complete the recommendations, design information is given also on sealing with a conventional O-ring, as well as guidelines for elevating a viewport in its flange.

Naval Civil Engineering Laboratory
STRUCTURAL DESIGN OF CONICAL ACRYLIC VIEWPORTS
(Final), by M. R. Snoey and M. G. Katona
TR-686 57 p. illus June 1970 Unclassified

1. Acrylic plastic viewports 2. Conical shape I. YF 38.535.005.01.005

The purpose of this report is to establish a rational engineering approach for the design of conical acrylic viewports. To achieve this goal, a time-dependent, yield-failure criterion was developed and utilized in the analysis of a variety of viewport configurations. Specifically, a range of thickness/minor diameter (t/d) ratios from 0.25 to 1.75 and included angles from 60° to 120° were analyzed by the finite element technique. Using the viewport structural analysis in conjunction with the yield-failure criterion for acrylic, time-dependent operating depths were determined as a function of viewport configuration. Paralleling the above, an experimental investigation was performed to validate the analytical results. Six full-scale viewports were tested for a year under simulated operational conditions that included simultaneous cycling of pressure and temperature, 0 to 4,000 psi and 70 to 35°F, respectively. Design recommendations are presented in the form of design curves which enable the design of a conical acrylic viewport for a specified operating pressure and duration under load. To complete the recommendations, design information is given also on sealing with a conventional O-ring, as well as guidelines for elevating a viewport in its flange.

Naval Civil Engineering Laboratory
STRUCTURAL DESIGN OF CONICAL ACRYLIC VIEWPORTS
(Final), by M. R. Snoey and M. G. Katona
TR-686 57 p. illus June 1970 Unclassified

1. Acrylic plastic viewports 2. Conical shape I. YF 38.535.005.01.005

The purpose of this report is to establish a rational engineering approach for the design of conical acrylic viewports. To achieve this goal, a time-dependent, yield-failure criterion was developed and utilized in the analysis of a variety of viewport configurations. Specifically, a range of thickness/minor diameter (t/d) ratios from 0.25 to 1.75 and included angles from 60° to 120° were analyzed by the finite element technique. Using the viewport structural analysis in conjunction with the yield-failure criterion for acrylic, time-dependent operating depths were determined as a function of viewport configuration. Paralleling the above, an experimental investigation was performed to validate the analytical results. Six full-scale viewports were tested for a year under simulated operational conditions that included simultaneous cycling of pressure and temperature, 0 to 4,000 psi and 70 to 35°F, respectively. Design recommendations are presented in the form of design curves which enable the design of a conical acrylic viewport for a specified operating pressure and duration under load. To complete the recommendations, design information is given also on sealing with a conventional O-ring, as well as guidelines for elevating a viewport in its flange.

Naval Civil Engineering Laboratory
STRUCTURAL DESIGN OF CONICAL ACRYLIC VIEWPORTS
(Final), by M. R. Snoey and M. G. Katona
TR-686 57 p. illus June 1970 Unclassified

1. Acrylic plastic viewports 2. Conical shape I. YF 38.535.005.01.005

The purpose of this report is to establish a rational engineering approach for the design of conical acrylic viewports. To achieve this goal, a time-dependent, yield-failure criterion was developed and utilized in the analysis of a variety of viewport configurations. Specifically, a range of thickness/minor diameter (t/d) ratios from 0.25 to 1.75 and included angles from 60° to 120° were analyzed by the finite element technique. Using the viewport structural analysis in conjunction with the yield-failure criterion for acrylic, time-dependent operating depths were determined as a function of viewport configuration. Paralleling the above, an experimental investigation was performed to validate the analytical results. Six full-scale viewports were tested for a year under simulated operational conditions that included simultaneous cycling of pressure and temperature, 0 to 4,000 psi and 70 to 35°F, respectively. Design recommendations are presented in the form of design curves which enable the design of a conical acrylic viewport for a specified operating pressure and duration under load. To complete the recommendations, design information is given also on sealing with a conventional O-ring, as well as guidelines for elevating a viewport in its flange.

Naval Civil Engineering Laboratory
STRUCTURAL DESIGN OF CONICAL ACRYLIC VIEWPORTS
(Final), by M. R. Snoey and M. G. Katona
TR-686 57 p. illus June 1970 Unclassified

1. Acrylic plastic viewports 2. Conical shape I. YF 38.535.005.01.005

The purpose of this report is to establish a rational engineering approach for the design of conical acrylic viewports. To achieve this goal, a time-dependent, yield-failure criterion was developed and utilized in the analysis of a variety of viewport configurations. Specifically, a range of thickness/minor diameter (t/d) ratios from 0.25 to 1.75 and included angles from 60° to 120° were analyzed by the finite element technique. Using the viewport structural analysis in conjunction with the yield-failure criterion for acrylic, time-dependent operating depths were determined as a function of viewport configuration. Paralleling the above, an experimental investigation was performed to validate the analytical results. Six full-scale viewports were tested for a year under simulated operational conditions that included simultaneous cycling of pressure and temperature, 0 to 4,000 psi and 70 to 35°F, respectively. Design recommendations are presented in the form of design curves which enable the design of a conical acrylic viewport for a specified operating pressure and duration under load. To complete the recommendations, design information is given also on sealing with a conventional O-ring, as well as guidelines for elevating a viewport in its flange.

Naval Civil Engineering Laboratory
STRUCTURAL DESIGN OF CONICAL ACRYLIC VIEWPORTS
(Final), by M. R. Snoey and M. G. Katona
TR-686 57 p. illus June 1970 Unclassified

1. Acrylic plastic viewports 2. Conical shape I. YF 38.535.005.01.005

The purpose of this report is to establish a rational engineering approach for the design of conical acrylic viewports. To achieve this goal, a time-dependent, yield-failure criterion was developed and utilized in the analysis of a variety of viewport configurations. Specifically, a range of thickness/minor diameter (t/d) ratios from 0.25 to 1.75 and included angles from 60° to 120° were analyzed by the finite element technique. Using the viewport structural analysis in conjunction with the yield-failure criterion for acrylic, time-dependent operating depths were determined as a function of viewport configuration. Paralleling the above, an experimental investigation was performed to validate the analytical results. Six full-scale viewports were tested for a year under simulated operational conditions that included simultaneous cycling of pressure and temperature, 0 to 4,000 psi and 70 to 35°F, respectively. Design recommendations are presented in the form of design curves which enable the design of a conical acrylic viewport for a specified operating pressure and duration under load. To complete the recommendations, design information is given also on sealing with a conventional O-ring, as well as guidelines for elevating a viewport in its flange.

Naval Civil Engineering Laboratory
STRUCTURAL DESIGN OF CONICAL ACRYLIC VIEWPORTS
(Final), by M. R. Snoey and M. G. Katona
TR-686 57 p. illus June 1970 Unclassified

1. Acrylic plastic viewports 2. Conical shape I. YF 38.535.005.01.005

The purpose of this report is to establish a rational engineering approach for the design of conical acrylic viewports. To achieve this goal, a time-dependent, yield-failure criterion was developed and utilized in the analysis of a variety of viewport configurations. Specifically, a range of thickness/minor diameter (t/d) ratios from 0.25 to 1.75 and included angles from 60° to 120° were analyzed by the finite element technique. Using the viewport structural analysis in conjunction with the yield-failure criterion for acrylic, time-dependent operating depths were determined as a function of viewport configuration. Paralleling the above, an experimental investigation was performed to validate the analytical results. Six full-scale viewports were tested for a year under simulated operational conditions that included simultaneous cycling of pressure and temperature, 0 to 4,000 psi and 70 to 35°F, respectively. Design recommendations are presented in the form of design curves which enable the design of a conical acrylic viewport for a specified operating pressure and duration under load. To complete the recommendations, design information is given also on sealing with a conventional O-ring, as well as guidelines for elevating a viewport in its flange.

Unclassified

Security Classification

**DOCUMENT CONTROL DATA - R & D**

*(Security classification of title, body of abstract and indexing annotation must be entered when the overall report is classified)*

1. ORIGINATING ACTIVITY *(Corporate author)*

Naval Civil Engineering Laboratory
Port Hueneme, California 93041

2a. REPORT SECURITY CLASSIFICATION

Unclassified

2b. GROUP

3. REPORT TITLE

STRUCTURAL DESIGN OF CONICAL ACRYLIC VIEWPORTS

4. DESCRIPTIVE NOTES *(Type of report and inclusive dates)*

Final; April 1967—April 1969

5. AUTHOR(S) *(First name, middle initial, last name)*

M. R. Snoey and M. G. Katona

| 6. REPORT DATE | 7a. TOTAL NO. OF PAGES | 7b. NO. OF REFS |
|---|---|---|
| June 1970 | 57 | 14 |

| 8a. CONTRACT OR GRANT NO. | 9a. ORIGINATOR'S REPORT NUMBER(S) |
|---|---|
| b. PROJECT NO. YF 38.535.005.01.005 | TR-686 |
| c. | 9b. OTHER REPORT NO(S) *(Any other numbers that may be assigned this report)* |
| d. | |

10. DISTRIBUTION STATEMENT

This document has been approved for public release and sale; its distribution is unlimited.

| 11. SUPPLEMENTARY NOTES | 12. SPONSORING MILITARY ACTIVITY |
|---|---|
| | Naval Facilities Engineering Command<br>Washington, D. C. 20390 |

13. ABSTRACT

The purpose of this report is to establish a rational engineering approach for the design of conical acrylic viewports. To achieve this goal, a time-dependent, yield-failure criterion was developed and utilized in the analysis of a variety of viewport configurations. Specifically, a range of thickness/minor diameter (t/d) ratios from 0.25 to 1.75 and included angles from 60° to 120° were analyzed by the finite element technique. Using the viewport structural analysis in conjunction with the yield-failure criterion for acrylic, time-dependent operating depths were determined as a function of viewport configuration.

Paralleling the above, an experimental investigation was performed to validate the analytical results. Six full-scale viewports were tested for a year under simulated operational conditions that included simultaneous cycling of pressure and temperature, 0 to 4,000 psi and 70 to 35°F, respectively.

Comparison of analytical and experimental results indicated excellent agreement for the physical location of viewport failure at specified loading histories.

Design recommendations are presented in the form of design curves which enable the design of a conical acrylic viewport for a specified operating pressure and duration under load. To complete the recommendations, design information is given also on sealing with a conventional O-ring, as well as guidelines for elevating a viewport in its flange.

DD FORM 1 NOV 65 1473 (PAGE 1)

S/N 0101-807-6801

Unclassified

Security Classification

| 14 KEY WORDS | LINK A | | LINK B | | LINK C | |
|---|---|---|---|---|---|---|
| | ROLE | WT | ROLE | WT | ROLE | WT |
| Acrylic plastic | | | | | | |
| Plexiglas | | | | | | |
| Undersea vehicles | | | | | | |
| Design curves | | | | | | |
| Habitats | | | | | | |
| Viscoelastic | | | | | | |
| Submersibles | | | | | | |
| O-ring seal | | | | | | |
| Finite element | | | | | | |
| Pressure cycling | | | | | | |
| Deep submergence | | | | | | |
| Stress analysis | | | | | | |
| Yield failure criterion | | | | | | |
| Windows | | | | | | |
| Failure theory | | | | | | |
| Hydrostatic pressure tests | | | | | | |
| Pressure vessels | | | | | | |
| Conical viewports | | | | | | |